Travelling waves in somitogenesis: collective cellular properties emerge from time-delayed juxtacrine oscillation coupling

ETH Zurich

Master's Thesis

Travelling waves in somitogenesis: collective cellular properties emerge from time-delayed juxtacrine oscillation coupling

Tomas Tomka

Supervisor: Dr. Marcelo Boareto
Professor: Prof. Dr. Dagmar Iber

Group: Computational Biology (CoBi)
Department of Biosystems Science and Engineering
Mattenstrasse 26, 4058 Basel, CH

handed in on May 15th, 2017

Abstract

The sculpturing of the vertebrate body plan into segments begins with the sequential formation of somites in the presomitic mesoderm (PSM). The rhythmicity of this process is controlled by travelling waves of gene expression which sweep across the PSM. These kinetic waves emerge from coupled cellular oscillators and travel in the direction of an increasing gradient of oscillation period. The oscillations are driven by autorepression of HES/HER genes and are synchronized via Notch signalling. These emergent properties have been studied in various models of increasing complexity. We design a reduced mechanistic model of the zebrafish PSM oscillator that recapitulates oscillator entrainments and travelling wave formation in the presence of spatiotemporal time delay gradients. Our model shows that three key parameters, the autorepression delay, the juxtacrine coupling delay, and the coupling strength, are sufficient to understand the emergence of the collective period, the collective amplitude, and the synchronization of neighbouring HES/HER oscillators. Our theoretical framework allows us to integrate and dissect key collective properties emerging from coupled oscillators. These emergent properties are likely to represent a fundamental principle governing also other developmental processes such as neurogenesis and angiogenesis.

Acknowledgements

First, I want to thank Dr. Marcelo Boareto, my supervisor, for his expertise, his enthusiasm in discussing new ideas, his constructive feedback, and his friendship. Equally thankful, I am for the opportunity, to be part of a great research group, and the support I received from Prof. Dr. Dagmar Iber.

In this thesis, when writing 'we', I refer to both, Dr. Marcelo Boareto and Prof. Dr. Dagmar Iber: Their valuable guidance and contribution lead to the draft of a research article accompanying this thesis. At the time of the Master's thesis submission, this draft is in the process of being submitted for publication.

Thanks to Dagmar Iber's endorsement, I had the pleasure to attended the Winter School on Quantitative Systems Biology in Triest and to philosophize on this occasion with Andrew Oates about somitogenesis, in December 2016.

As well, I want to thank all the other members of the CoBi group for the enjoyable time spent together.

Most importantly, I am grateful to my family and my closest friends. And I am deeply thankful for the people who took a stand for me on my educational path - especially for the unconditional support of my mother.

Key vocabulary

Angiogenesis	The formation of new blood vessels in the developing embryo.
Autonomous oscillator	An uncoupled cellular oscillator.
Autorepression	An autorepressive gene codes for a protein that represses the same gene within the same cell. Time-delayed autorepression can drive cellular oscillators. (Lewis, 2003; Monk, 2003; Novak & Tyson, 2008)
Cellular oscillator	A cell with periodically oscillating expression of a certain gene and cyclic levels of the corresponding mRNA and protein.
Cell-based model	A model of the collective behaviour of individual cells and their physical and/or biological interactions.
Coupling	Communication between neighbouring oscillators. This leads to adjustment of the individual oscillatory dynamics to a collective period and amplitude. Coupling affects the synchronization behaviour. (Morelli *et al.*, 2009; Oates *et al.*, 2012)
Delay equation	Differential equations which incorporate explicit time delays. During numerical simulations, the (partial) history of the system is stored and affects the output of the next iteration. Can be used to model e.g. time-delayed autorepression. (Novak & Tyson, 2008)
Dynamic salt-and-pepper patterning	Tissue-wide pattern arising from anti-synchronization between neighbouring cells (Kageyama *et al.*, 2008).
Juxtacrine signalling	Biological transmission of information from a sending cell to a neighbouring receiving cell via interaction of a membrane-bound ligand and receptor (e.g. Notch signalling).
HES/HER genes	An autorepressive gene family, which drives the cellular oscillators in the PSM (Oates & Ho, 2002; Bessho *et al.*, 2003; Lewis, 2003; Monk, 2003).
Kinematic wave	A travelling wave without mass transport. The wave emerges from static components with periodically changing states (Oates *et al.*, 2012). An example is the wave performed by the audience in a sports stadium.

Mechanistic model	In systems biology, the components of a mechanistic model represent molecular species, which interact with each other through kinetic reactions.
Neurogenesis	The embryonic process where neural stem cells give rise to all the neurons of the developing central nervous system (Götz & Huttner, 2005).
Notch signalling	A juxtacrine signalling pathway, which couples neighbouring HES/HER oscillators in the PSM. The ligand (e.g. Delta) on the membrane of the signal sending cell activates the Notch receptor on the membrane of the signal receiving cell. (Andersson *et al.*, 2011)
Presomitic mesoderm (PSM)	The embryonic tissue which will differentiate into somites at its anterior boundary during somitogenesis. The posterior PSM is continuous with the tail bud. (Oates *et al.*, 2012)
Reduced model	A model which explicitly does not describe the process in the entire complexity that is suggested by the current state of knowledge. It aims at identifying the fundamental principles that govern the process. (Hermanns *et al.*, 2016)
Scaling	The phenomenon that biological patterns and structures are built proportional to a reference size. This reference size is usually the body size or the size of the patterned tissue domain. Scaled relationships can be drawn across developmental time (e.g. in a growing tissue) and/or across a population of individuals. (Barkai & Shilo, 2013; Vollmer *et al.*, 2017)
Somitogenesis/Somites	Somites are precursors of the repetitive body segments consisting of vertebrae and their associated muscles, occurring in vertebrates. Somitogenesis is the embryonic developmental process that gives rise to somites, which are formed from the PSM. (Oates *et al.*, 2012; Hubaud & Pourquié, 2014)
Synchronization behaviour	Coordination of oscillation phases in neighbouring oscillators with a common period mediated by coupling. In-phase patterns lead to synchrony, while phase differences of half of the common period lead to anti-synchrony. (Pikovsky *et al.*, 2001)
Tail bud	The posterior region where the tail structures grow in the developing zebrafish embryo (Oates *et al.*, 2012).
Time delay	Biological processes are not instantaneous. Processes can be slow when they depend on elementary events with a low likelihood; these processes can be modelled with kinetic rates ('soft' time delay). But there are processes, e.g. when information has to cross physical space, that are delayed for every elementary event (resembling a conveyor belt). Such explicit ('hard') time delays can be modelled with delay equations (Novak & Tyson, 2008).

Trans-repression A certain gene represses the same gene in a neighbouring cell through juxtacrine signalling. This term is currently not well-established in the field and not to be confused with `https://en.wikipedia.org/wiki/Transrepression`.

Travelling wave A wave in which phase values (e.g. peaks of amplitudes) travel through the medium.

Zebrafish A tropical freshwater fish, *danio rerio*, which is a convenient vertebrate model organism because of its transparency (Spence *et al.*, 2007). It is also known for its regenerative capabilities (Goldshmit *et al.*, 2012).

Contents

1. Introduction

The body axis of vertebrates is segmented into anatomical modules consisting of vertebrae and their associated muscles. This segmentation has a key role in defining the mode of locomotion of an animal (Ward & Mehta, 2011). The embryonic precursors of the segments are called somites. The bilateral symmetric pairs of somites form in a process referred to as somitogenesis (Oates *et al.*, 2012; Hubaud & Pourquié, 2014). At the same time as somitogenesis proceeds, the body axis is elongated posteriorly at the so-called tail bud by proliferation of presomitic mesoderm (PSM) cells originating from the marginal zone in zebrafish and frogs or the primitive streak in chicken and mice. Periodically, a pair of somites buds off from the anterior end of the PSM, which lies on both sides of the neural tube. In zebrafish, a new pair of somites is formed in the anterior trunk constantly every 23 min at 28.5 °C until this rhythm is gradually slowed down during the tail segmentation (Schröter *et al.*, 2008). The rhythmicity is controlled by travelling waves of gene expression which sweep from the tail bud to the anterior end of the PSM (Palmeirim *et al.*, 1997). The travelling waves emerge from the coordinated oscillation in individual cells (Jiang *et al.*, 2000). In the following, we will first discuss a well-established theoretical model of somitogenesis, the clock-and-wavefront model. We will then in detail report what is known about the individual cellular oscillator, the coupling between neighbouring cells and the emergence of the travelling waves.

1.1. Rhythmical formation of somites: clock and wavefront

The most widely accepted model for the sequential formation of somites is the clock-and-wavefront model (Cooke & Zeeman, 1976; Oates *et al.*, 2012; Hubaud & Pourquié, 2014). It postulates that cells located at the anterior boundary of the PSM, the wavefront, undergo an abrupt change in cellular properties triggered by a periodic segmentation signal of the clock (Cooke & Zeeman, 1976). This clock, the first component of the model, has been shown to entail the oscillatory expression of genes involved in the Notch, WNT and FGF signalling pathways (Palmeirim *et al.*, 1997; Dequeant *et al.*, 2006). The most prominent examples are genes of the HES/HER family (Palmeirim *et al.*, 1997; Cooke, 1998; Bessho *et al.*, 2003). The oscillations in HES/HER were shown to be based on time-delayed autorepression, where the time delay originates from mRNA splicing and nuclear export processes (Lewis, 2003; Monk, 2003; Takashima *et al.*, 2011; Hoyle & Ish-Horowicz, 2013). In principle, the oscillations in individual cells are synchronized perpendicularly to the body axis, such that they form travelling waves propagating in the anterior direction (Oates *et al.*, 2012; Hubaud & Pourquié, 2014). Strictly, the bilateral symmetric travelling waves acquire a folded shape in zebrafish, termed a chevron, which is thought to arise from mechanical forces (Rost *et al.*, 2014). The underlying synchronicity of neighbouring HES/HER oscillators is mediated by juxtracrine Notch signalling (Jiang *et al.*, 2000; Lewis, 2003; Liao & Oates, 2016) and is discussed below (Section 1.2).

The second component of the clock-and-wavefront model, the wavefront, has been hypothesised to be defined via a threshold in the FGF or WNT gradients, which decline towards

the anterior end of the PSM (Dubrulle *et al.*, 2001; Sawada *et al.*, 2001; Aulehla *et al.*, 2003, 2008; Dunty *et al.*, 2008; Naiche *et al.*, 2011; Bajard *et al.*, 2014). The FGF signalling gradient forms because the corresponding ligand-expressing gene fgf8 is transcribed only in the tail bud and its mRNA is gradually decaying in the presomitic cells that are left behind by the proliferating tail bud (Dubrulle & Pourquié, 2004). More generally, this is referred to as a 'gradient by inheritance' - established by simultaneous cell flow and ligand mRNA or protein decay - and such a mechanism is thought to also govern the graded expression of wnt3A in the PSM (Aulehla & Pourquié, 2010; Bajard *et al.*, 2014). Due to continuous axis elongation, the source of the ligand in the tail bud is progressively drawn further away from the anterior. The wavefront, presumably specified by a threshold in one of these gradients, is shifted accordingly. An opposing retinoic acid gradient shows highest concentration in the somites and is thought to antagonize the FGF gradient by mutual inhibition (Niederreither *et al.*, 1997; Diez del Corral *et al.*, 2003; Goldbeter *et al.*, 2007; Jörg *et al.*, 2016).

According to the clock-and-wavefront model, segmentation is initiated when the clock signal reaches the moving wavefront (Cooke & Zeeman, 1976). This leads to a transition of the synchronized presomitic cell patches to distinct blocks of epithelial cells, the somites, that bud off from the PSM (Saga, 2012). The MESP genes are essential in triggering this mesenchymal-to-epithelial transition (Saga *et al.*, 1997; Takahashi *et al.*, 2000; Sawada *et al.*, 2000). In mice, Mesp2 has been linked to both, the clock and wavefront, being positively regulated by Notch and negatively regulated by FGF signalling (Yasuhiko *et al.*, 2006; Oginuma *et al.*, 2008; Naiche *et al.*, 2011). In zebrafish, expression of MESP genes seems to be similarly controlled by the wavefront, but the connection to the clock remains unclear (Sawada *et al.*, 2001; Bajard *et al.*, 2014; Wanglar *et al.*, 2014; Yabe & Takada, 2016).

1.2. Architecture and synchrony of coupled HER oscillators

The autorepressive HES and HER genes lie at the core of the segmentation clock in mice and zebrafish, respectively. These genes encode basic helix loop helix (bHLH) transcriptional repressors. In zebrafish, which serves us as a biological model organism, either of the two proteins Her1 and Her7 represses both corresponding genes in a redundant manner (Oates & Ho, 2002; Henry *et al.*, 2007; Giudicelli *et al.*, 2007). Another bHLH factor gene, hes6, is expressed in an FGF-dependent posterior-to-anterior gradient in the PSM (Kawamura *et al.*, 2005). Together Her1, Her7 and Hes6 span a topology of homo- and heterodimers, of which only Her1:Her1 and Her7:Hes6 are active repressors, targeting the promoters of *her1*, *her7* and *deltaC* (Schröter *et al.*, 2012). The latter is the link that couples neighbouring oscillators: due to periodic repression by active Her dimers, *deltaC* is expressed cyclically and activates the HER genes in neighbouring cells via Notch signalling (Jiang *et al.*, 2000; Lewis, 2003; Liao & Oates, 2016). PSM cells have been shown to oscillate autonomously when uncoupled or isolated, although with a lower precision and persistence (Maroto *et al.*, 2005; Masamizu *et al.*, 2006; Webb *et al.*, 2016).

The fact that the cells of the PSM synchronize their oscillations perpendicular to the direction of propagation of the travelling waves is intriguing. This synchronization requires cell-cell contact and is mediated by the coupling via Notch signalling (Jiang *et al.*, 2000; Maroto *et al.*, 2005; Horikawa *et al.*, 2006; Riedel-Kruse *et al.*, 2007; Özbudak & Lewis, 2008). However, it has been shown that the synchrony is initiated in the presumptive mesoderm ring independently of Notch signalling (Riedel-Kruse *et al.*, 2007). In Notch pathway mutants, a

few intact anterior somites are formed, but as segmentation proceeds to the posterior, severe defects occur (Jiang *et al.*, 2000). The widely-supported desynchronization hypothesis has been founded on this observation and states that the only role of Notch signalling is to maintain the initial synchrony (Jiang *et al.*, 2000; Riedel-Kruse *et al.*, 2007; Özbudak & Lewis, 2008; Liao & Oates, 2016).

Theoretical models show that trans-repression can lead to either synchronization or salt-and-pepper pattern of oscillation phases, depending on the time delay involved in trans-repression (Lewis, 2003; Tiedemann *et al.*, 2007; Ay *et al.*, 2013). This time delay is dominated by the translational delay of DeltaC, which has been measured to be approximately 30 min at 28 °C (Giudicelli *et al.*, 2007). Mathematical formulations show that the collective period of coupled oscillators might differ from the period of uncoupled oscillators, depending in a non-trivial way on both, the coupling strength and the coupling delay (Niebur *et al.*, 1991; Morelli *et al.*, 2009; Herrgen *et al.*, 2010; Wang *et al.*, 2014). In the PSM, the collective period is a local property and related measurements are discussed below (Section 1.3; Fig. 1.1).

DeltaD, another ligand of the Notch pathway, is not expressed cyclically but in a decreasing gradient from posterior to anterior (Holley *et al.*, 2002; Mara *et al.*, 2007; Wright *et al.*, 2011). In contrast to DeltaC, DeltaD is thought to cis-inhibit Notch (Matsuda & Chitnis, 2009). It has been suggested that DeltaD, unable to activate Notch by itself, could potentiate trans-repression via DeltaC by heterodimerization (Wright *et al.*, 2011).

1.3. Travelling waves of genetic expression

In zebrafish, the most prominent cyclically expressed genes that constitute the travelling wave are *her1*, *her7* and *deltaC* (Krol *et al.*, 2011; Oates *et al.*, 2012). From the posterior to the anterior, the travelling wave is slowing gradually while its wavelength decreases (Palmeirim *et al.*, 1997; Giudicelli *et al.*, 2007; Fig. 1.1). Initially, the clock-and-wavefront model was thought to entail a genetic oscillator with a single, well-defined period that governs the rhythmicity of the segmentation clock (Cooke & Zeeman, 1976; Oates *et al.*, 2012). This simplistic picture has since been revisited with emphasis on the distinction between different notions of periods involved in the process.

On a tissue level, one observes that the segmentation or somitogenesis period, the period with which the somites are formed, is equivalent to the period at which the travelling waves reach the wavefront (Soroldoni *et al.*, 2014). The segmentation is accelerated compared to the frequency at which travelling waves exit the tailbud due to a Doppler effect: relative to the tailbud, the anterior boundary is moving towards the approaching travelling waves and thus registers an increased frequency of wave signals (Soroldoni *et al.*, 2014; Fig. 1.1). In vivo, the PSM shortens non-linearly and therefore the wave pattern does not scale in time. Consequently, a steady-state description of this process, where the proliferation rate equals the segmentation rate, is not adequate (Soroldoni *et al.*, 2014; Jörg *et al.*, 2015).

The somitogenesis period is lengthened by the autorepression delay, as well as shortened in zebrafish or lengthened in mouse by Notch signalling (Harima *et al.*, 2013; Kim *et al.*, 2011; Herrgen *et al.*, 2010; Liao *et al.*, 2016). The accelerating Doppler effect on the somitogenesis period is decreased by the so-called Dynamical Wavelength effect, the shortening of the wavelength of the travelling wave in time (Soroldoni *et al.*, 2014; Jörg *et al.*, 2015). The size of the forming somite, referred to as $S0$, has been determined to be half of the wavelength at the PSM-somite border; the formation of $S0$ is completed when a full period of oscillation is

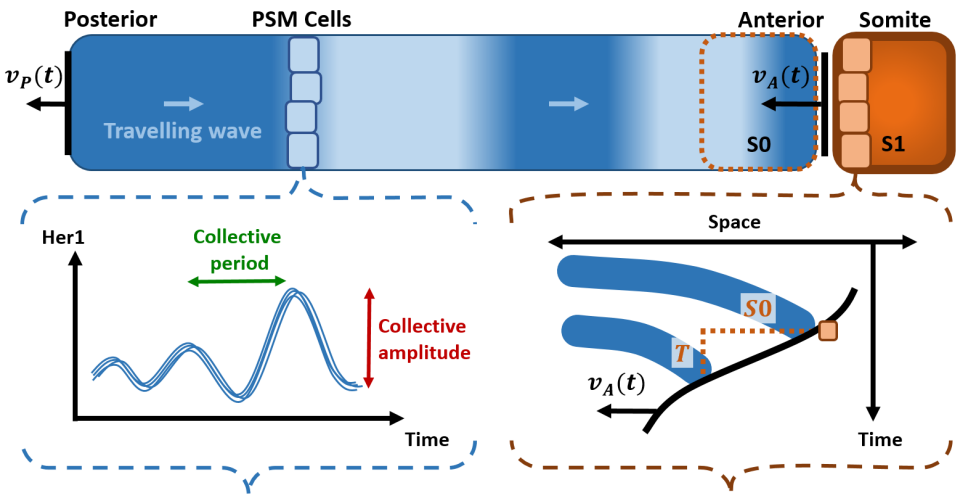

Figure 1.1.: **Schematic representation of somitogenesis from the reference frame of individual cells.** The anterior boundary of the PSM approaches the cells faster than the posterior boundary recedes due to proliferation; satisfying $v_A(t) > v_P(t)$ during the entire process (Soroldoni *et al.*, 2014). This leads to a shrinkage of the PSM over time (Soroldoni *et al.*, 2014). Consequently, a Doppler effect is experienced at the anterior boundary when receiving the signal of the travelling wave (Soroldoni *et al.*, 2014). The individual cellular oscillators will synchronize perpendicularly to the travelling wave direction, attaining a collective period and amplitude of cyclic components such as Her1. Both, the collective period and amplitude, increase as the anterior boundary is approaching (bottom left; Delaune *et al.*, 2012; Shih *et al.*, 2015). The forming somite's size $S0$, the somitogenesis period T and the velocity of the anterior boundary v_A are interdependent (bottom right; Jörg *et al.*, 2015).

cycled at this border (Shih *et al.*, 2015; Fig. 1.1). Given a local estimate for the velocity of the anterior PSM boundary $\tilde{v}_A$, the somite size S is approximated as $S \approx \tilde{v}_A T$, where T is the somitogenesis period (Jörg *et al.*, 2015; Fig. 1.1, bottom right). There is also evidence suggesting that somite size is linked to the phase gradient (Lauschke *et al.*, 2013; Shih *et al.*, 2015). However, the mechanism of oscillation arrest in $S0$ remains elusive (Shih *et al.*, 2015; Jörg *et al.*, 2015). Furthermore, the segmentation scales with the body size (Cooke, 1975; Tam, 1981). Scaling of somite size, oscillation phase and travelling wave velocity has also been recently reported to occur during an *ex vivo* segmentation process, but the mechanism remains unknown (Lauschke *et al.*, 2013). *In vivo*, somite size is a non-linear function of time and therefore does not scale similarly (Jörg *et al.*, 2015). I introduce *ex vivo* scaling, sketch possible mechanisms at work, and discuss biological hypotheses, separately in Appendix A.3.

1.4. Individual cell dynamics induce travelling wave formation

On the level of an individual cellular oscillator, single cell analyses reveal that both, the locally collective period and amplitude of Her1, are increasing as the cell is flowing across the

PSM (Delaune *et al.*, 2012; Shih *et al.*, 2015; Fig. 1.1). Several computational models show that in the presence of such a gradient in oscillation period, travelling waves emerge (Kærn *et al.*, 2000; Jaeger & Goodwin, 2001; Tiedemann *et al.*, 2007; Uriu *et al.*, 2009; Ay *et al.*, 2014). Mechanistically, a gradient in oscillation period, and therefore travelling waves, can be established by imposing a gradient of a model parameter, such as intronic delays or degradation rates (Tiedemann *et al.*, 2007; Uriu *et al.*, 2009; Ay *et al.*, 2014). Hypothetically, such a reaction rate could be regulated by paracrine signalling, namely the FGF/WNT gradient present in the PSM. Because single-cell data is scarce and reaction rate estimates broad, these models still lag in accuracy behind non-mechanistic descriptions, which for instance can approximate somite size reasonably well (Morelli *et al.*, 2009; Herrgen *et al.*, 2010; Jörg *et al.*, 2015, 2016).

1.5. State of the field and contribution of the thesis

In summary, the travelling waves observed in the PSM carry a repetitive segmentation signal, which is read out at the moving wavefront (Oates *et al.*, 2012; Hubaud & Pourquié, 2014; Soroldoni *et al.*, 2014; Shih *et al.*, 2015). The formation of these travelling waves is based on three main principles: the oscillation of autorepressive HES/HER genes (Palmeirim *et al.*, 1997; Cooke, 1998; Bessho *et al.*, 2003; Lewis, 2003; Monk, 2003), the local synchronization of neighbouring HER/HES oscillators via Notch signalling (Jiang *et al.*, 2000; Lewis, 2003; Giudicelli *et al.*, 2007; Liao & Oates, 2016), and an increasing gradient of oscillation period, which defines the direction of propagation of the travelling wave (Kærn *et al.*, 2000; Jaeger & Goodwin, 2001; Tiedemann *et al.*, 2007; Uriu *et al.*, 2009; Ay *et al.*, 2014). Each of these principles has been studied in different mechanistic models of largely varying complexity (Lewis, 2003; Monk, 2003; Tiedemann *et al.*, 2007; Uriu *et al.*, 2009; Hester *et al.*, 2011; Ay *et al.*, 2014).

Here, we develop a reduced mechanistic model that can account for the three principles mentioned above. For that, we revisit a simple model of the zebrafish *her1* oscillator proposed by Julian Lewis (Lewis, 2003). Lewis used both, the *her1* and the *her7* oscillator to couple neighbouring cells via deltaC (Lewis, 2003). In contrast, we couple only the *her1* oscillators, similarly as previously done in analytical studies (Wang *et al.*, 2014), but our model incorporates only two time delays, instead of three. Using this reductive approach, we can recapitulate the principles that govern the travelling wave. We find that both, the dynamics of the individual cellular oscillator and the synchronization of neighbouring PSM cells, are modulated by three key parameters of the model: the HES/HER autorepression delay, the intercellular coupling delay, and the coupling strength between neighbouring cells. These insights allow us to discuss the general role of Notch-mediated oscillation coupling in differentiation processes involved not only in somitogenesis, but also in other developmental processes such as neurogenesis and angiogenesis.

2. Methods

2.1. A reduced model of the zebrafish *her1* oscillator

The travelling waves occurring in the PSM are induced by the dynamics of individual cellular oscillators (Tiedemann *et al.*, 2007; Uriu *et al.*, 2009; Ay *et al.*, 2014). The basis of a computational model of the travelling wave is therefore the cellular oscillator, which is driven by two negative feedback loops in zebrafish, one over the Her1 homodimer and one over the Her7:Hes6 heterodimer (Schröter *et al.*, 2012). The two loops are thought to be redundant and the *her7;hes6* double mutant is segmented normally in most cases (Schröter *et al.*, 2012). A reduced model, incorporating the autorepressive loop of *her1* only, should therefore be capable, in principle, to represent the PSM oscillator adequately. A mathematical representation of this reduced model of the uncoupled, or autonomous, zebrafish oscillator has been proposed as two delayed differential equations (Lewis, 2003; Fig. 2.1):

$$\dot{p}(t) = am(t-\tau_p) - bp(t) \tag{2.1}$$

$$\dot{m}(t) = k\overbrace{H^-(p(t-\tau_m), n_A, p_0)}^{\text{autorepression}} - cm(t) \tag{2.2}$$

The two components of the model are the cytosolic mRNA, m, and the nuclear protein, p, of Her1. The nuclear protein is produced at a translation rate $a = 4.5\,\text{min}^{-1}$ and degraded at a rate $b = 0.23\,\text{min}^{-1}$ (Lewis, 2003). The transcription rate is given by $k = 33\,\text{min}^{-1}$ and the mRNA is degraded at $c = 0.23\,\text{min}^{-1}$, the same degradation rate as for the protein (Lewis, 2003). A negative Hill function H^- (see Eq. (A.1)) is used to model autorepression, with a Hill constant $p_0 = 40$ and a Hill coefficient $n_A = 2$. The translational and transcriptional delays have been estimated to be $\tau_p \approx 2.8\,\text{min}$ and $\tau_m \approx 10\,\text{min}$, respectively (Lewis, 2003; Hanisch *et al.*, 2013).

Additionally, we couple neighbouring oscillators by trans-repression, representing Notch signalling (Eqs. (2.3) and (2.4); Fig. 2.1).

$$\dot{p}(t) = am(t) - bp(t) \tag{2.3}$$

$$\dot{m}(t) = k\overbrace{H^-(p(t-\tau_A), n_A, p_0)}^{\text{autorepression}}\overbrace{((1-\epsilon) + \epsilon H^-(p_{\text{ext}}(t-\tau_C), n_C, p_0))}^{\textit{trans}\text{-repression}} - cm(t) \tag{2.4}$$

Different coupling mechanisms have been introduced, including very similar formulations (Lewis, 2003; Tiedemann *et al.*, 2007; Kim *et al.*, 2010; Wang *et al.*, 2014). Lewis himself coupled neighbouring oscillators consisting of both, a *her1* and a *her7* circuit, and represented *deltaC* explicitly (Lewis, 2003). The transcription is repressed by the Notch signal, which depends in our model on the average Her1 concentration in neighbouring cells p_{ext}. Again, we use a negative Hill function to model trans-repression, with a Hill constant $p_0 = 40$ and a

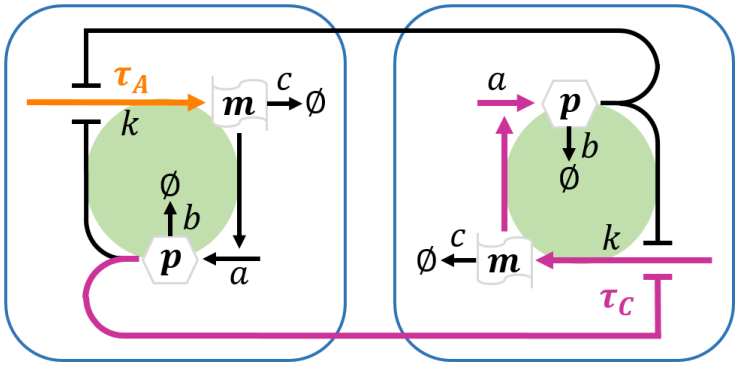

Figure 2.1.: **Graphical representation of the reduced model for the cellular oscillators in the PSM.** Each cell contains a loop over the autorepressive protein, p, and its mRNA, m, with an autorepression delay τ_A, which delays mRNA transcription. The oscillators are coupled between neighbours by trans-repression with a coupling delay τ_C. This coupling delay represents the time needed to transmit the phase information between cyclic protein levels in neighbouring cells. The model is mathematically described by Eqs. (2.3) and (2.4).

Hill coefficient $n_C = 1$. We introduced the parameter $\epsilon \in [0, 1]$ to regulate coupling strength; as a default, we use maximal coupling, $\epsilon = 1$. We also summarize the transcriptional and translational delays into one autorepression delay τ_A, rendering the model more abstract, but simpler to understand. The default value $\tau_A = 10\,\text{min}$ deviates from the sum $\tau_p + \tau_m \approx 12.8\,\text{min}$ moderately and yields good synchronization results. The expression of deltaC is delayed by translational and transcriptional delays, which have been measured to be roughly 30 min and 10 min, respectively, resulting in a total deltaC expression delay $\tau_D \approx 40\,\text{min}$ (Giudicelli *et al.*, 2007; Hanisch *et al.*, 2013). The juxtacrine signalling delay via Notch, referred to as the coupling delay, is defined as

$$\tau_C = \tau_A + \tau_D \tag{2.5}$$

Consequently, its duration is approximated as $\tau_C \approx 50\,\text{min}$.

The zebrafish segmentation process is sensitive to body size and temperature (Cooke, 1975; Tam, 1981; Schröter *et al.*, 2008). Additionally, the somitogenesis period of the *her7;hes6* double mutant is slower relative to the wild type (Schröter *et al.*, 2012). Therefore, although the reductive approach of our model allows us to make conceptual conclusions, quantitative predictions are not advised.

Additional considerations, which lead us to the selection of the model described above, are found in the Appendix A.2.

2.2. Cell-based simulations

The delay equations (Eqs. (2.3) and (2.4)) are computationally solved using Pydelay (Flunkert & Schoell, 2009). To approximate the PSM locally, we use 4×4 cell patches on a quadratic lattice with periodic boundary conditions and homogeneous parameter values, similarly to previous studies (Tiedemann *et al.*, 2007; Ay *et al.*, 2013). We calculate the oscillation properties after the cells have reached a stable oscillating state. To measure synchronization

of Her1 protein levels across such a tissue, we take the average pairwise Pearson's r coefficient of Her1 concentration trajectories among all cells of the tissue. The corresponding value lies between -1, for perfect anti-synchronization, and 1, for perfect synchronization. The noise is implemented using the method provided by Pydelay (Flunkert & Schoell, 2009) and the Gaussian white noise of unit variance is scaled additionally with the maximum concentration observed in the oscillation of the corresponding model component (protein or mRNA).

To simulate travelling waves in the PSM, we use a cylindrical domain of 4×4 cells on a quadratic lattice and induced parameter value inhomogeneity across the cylinder height spanning 50 cells, which represents the anterior-posterior axis. For simulations on dynamic domains we adopt the approach of Ay *et al.* (2014): Firstly, we simulated 4×20 cells for 84 min. This domain represents the tail bud, which we assume to be homogeneous in parameter values, with a common period (Oates *et al.*, 2012). Secondly, we divide the 4 posterior-most cells every 6 min for 150 min, until the entire 4×50 cell domain is filled (Ay *et al.*, 2014). After a cell exits the tail bud, the time delay parameters increase every 6 min as it moves toward the anterior boundary (as suggested by the results described below). Thirdly, we model continuous cell flow, by additionally removing the 4 anterior-most cells every 6 min (Ay *et al.*, 2014). Note, that such a steady-state cell flow is a simplifying assumption and does not allow for quantitative descriptions of the travelling wave (Soroldoni *et al.*, 2014; Jörg *et al.*, 2015).

The Python code is available on GitHub (see Appendix A.4).

3. Results

3.1. The autorepression delay in autonomous HES/HER oscillations

The HES and HER genes drive the PSM oscillator in mice and zebrafish, respectively. Numerical and analytical results show that the period of the autonomous HES/HER oscillator depends on the autorepression delay and the protein and mRNA half-lives (Fig. A.1; Lewis, 2003; Monk, 2003; Hori *et al.*, 2013). In our model, when the autorepression delay of *her1*, τ_A, is lengthened, both, the autonomous period and amplitude increase (Fig. 3.1). There is a lower limit $\tau_A \approx 7.5\,\text{min}$ for the existence of oscillations, which depends on the kinetic rates and the Hill coefficient (Fig. 3.1A; Hori *et al.*, 2013; Novak & Tyson, 2008).

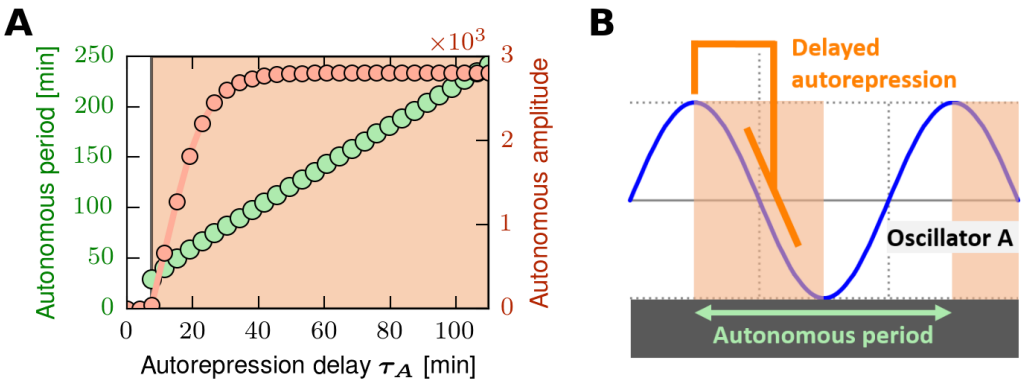

Figure 3.1.: The autorepression delay can modulate the period and amplitude in an autonomous Her1 oscillator. (A) The period and amplitude of autonomous oscillations depend on the autorepression delay; values represent averages over 4×4 cells. (B) A simple thought experiment relates the autorepression delay and the autonomous period of the Her1 oscillator. An increase of the autorepression delay expands the orange region, where Eq. (3.1) is satisfied, because the maximal repression signal takes longer to shut-down *her1* expression, which leads to a longer oscillation period.

To understand the effect of the autorepression delay intuitively, we follow a simple thought experiment (Fig. 3.1B): To maintain the oscillation, the autorepression of an oscillator must peak in the phase where the oscillation amplitude is decreasing. Therefore, for oscillatory curves that are symmetric in peaks and troughs, such as sinusoidal functions, with a period T_a, the autorepression delay τ_A satisfies:

$$\tau_A \in [kT_a, (k + \frac{1}{2})T_a] \text{ with } k \in \mathbb{N} \tag{3.1}$$

If the autorepression delay τ_A is lengthened, starting at a peak, it will take longer to repress *her1* expression maximally and reach the oscillation trough. Consequently the autonomous period T_a lengthens, such that the condition is still satisfied (Figure 3A).

3.2. Juxtacrine coupling controls cell-cell synchronization and robustness against noise

Riedel-Kruse *et al.* (2007) proposed that an initial synchrony of the cellular HER oscillators is established in the presumptive mesoderm by simultaneous gene induction. In Notch pathway mutants, where oscillations are thought be autonomous, this synchrony is lost gradually (Jiang *et al.*, 2000; Riedel-Kruse *et al.*, 2007; Özbudak & Lewis, 2008; Liao & Oates, 2016). In our model, by setting all initial concentrations to zero and starting expression in all cells simultaneously, we observe a first peak of Her1 oscillation that is massively increased relative to the consecutive peaks, because the system initially has no memory of autorepression (Fig. 3.2A). As time goes, in the absence of intercellular coupling, the autonomously oscillating cells lose their synchrony due to noise (Fig. 3.2A).

In the wild type, autonomous oscillators are coupled via Notch signalling, which increases robustness of synchronization (Jiang *et al.*, 2000; Riedel-Kruse *et al.*, 2007; Özbudak & Lewis, 2008; Soza-Ried *et al.*, 2014; Jenkins *et al.*, 2015; Liao & Oates, 2016). To investigate the effect of cell-cell coupling, we simulated a tissue of cells with different levels of noise and coupling strength, and we confirm that coupling increases the robustness of synchronization, i.e. it renders the synchronization less sensitive to noise (Fig. 3.2B). We further simulated how sudden coupling coordinates oscillators which lost their synchrony in presence of noise (Fig. 3.2C,D). Consistent with previous studies (Lewis, 2003; Tiedemann *et al.*, 2007; Morelli *et al.*, 2009; Herrgen *et al.*, 2010), we observe that the cells either synchronize (Fig. 3.2C) or anti-synchronize (Fig. 3.2D), depending on the value of the coupling delay. On a tissue level, the latter is also referred to as dynamic salt-and-pepper patterning and has been proposed to regulate the maintenance of neural progenitors during brain development (Shimojo *et al.*, 2008; Kageyama *et al.*, 2008).

Taken together, we observe in our model that the strength of juxtacrine coupling is determining the robustness of cell-cell synchronization, while the delay of this coupling is determining whether expression of her1 in neighbouring cells is synchronized or anti-synchronized. In the following section, we examine how exactly the coupling delay influences the collective behaviour of *her1* oscillators.

3.3. The coupling delay critically modulates collective oscillatory dynamics

In our model, we observe alternating regions of synchronization and anti-synchronization for a range of coupling delays τ_C (Fig. 3.3; for exemplary simulations see Fig. 3.2C,D). In each region, the collective period increases monotonically (Fig. 3.3A) and the collective amplitude describes a parabola with a local maximum (Fig. 3.3B). A similar pattern has been reported partially in the context of the zebrafish PSM oscillator, HES/HER oscillations in neural differentiation, and a variety of synchronization phenomena across the natural sciences (Wang *et al.*, 2014; Morelli *et al.*, 2009; Herrgen *et al.*, 2010; Momiji & Monk, 2009; Sadeghi &

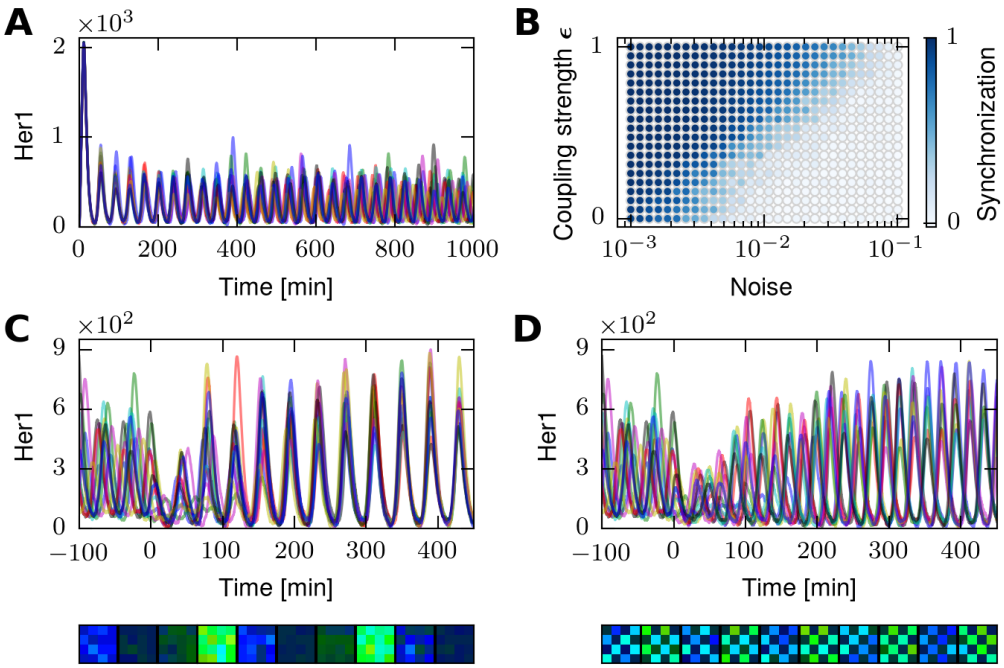

Figure 3.2.: **Coupling leads to robust cell-cell synchronization or dynamic salt-and-pepper patterning.** (A) Simultaneous onset of *her1* expression leads to synchrony, which is lost over time in the absence of coupling. (B) Stronger coupling renders synchronization more robust, i.e. less sensitive to noise (average over 5 replicates). (C, D) At the endpoint of (A) which is now referred to as timepoint 0, the cells are coupled with coupling delays (C) $\tau_C \approx 50\,\text{min}$ (default value) or (D) $\tau_C \approx 30\,\text{min}$. The spatial patterns are displayed (bottom) for the last 90 minutes of the corresponding concentration trajectories (top). The noise level in (C, D) corresponds to the value of 10^{-2} in (B); see Section 2.2 for details. All data has been recorded for 4×4 cell patches.

Valizadeh, 2014; Pavlides *et al.*, 2015; Vanag *et al.*, 2016; Wetzel *et al.*, 2017). In contrast to other mathematical descriptions, however, we do not observe oscillation death, a stable non-oscillating state, which has been hypothesized to occur between the synchronization and anti-synchronization phase space regions (Fig. 3.3B, Shimojo *et al.*, 2016).

Again, to understand the behaviour intuitively, we propose a thought experiment (Fig. 3.3C, left). Suppose two synchronized oscillators A and B with a collective period T_c that mutually repress each other. They will maintain synchrony only if trans-repression of B by A peaks within the oscillation phase of B where the amplitude is decreasing, and vice versa. Based on that, a relation between the common coupling delay τ_C and the collective period T_c analogous to Eq. (3.1) can be formulated — for oscillatory curves that are symmetric in peaks and troughs synchronized oscillators satisfy:

$$\tau_C \in [kT_c, (k + \frac{1}{2})T_c] \text{ with } k \in \mathbb{N} \tag{3.2}$$

Conversely, if this condition is not satisfied, the oscillators will adjust their phases, such that

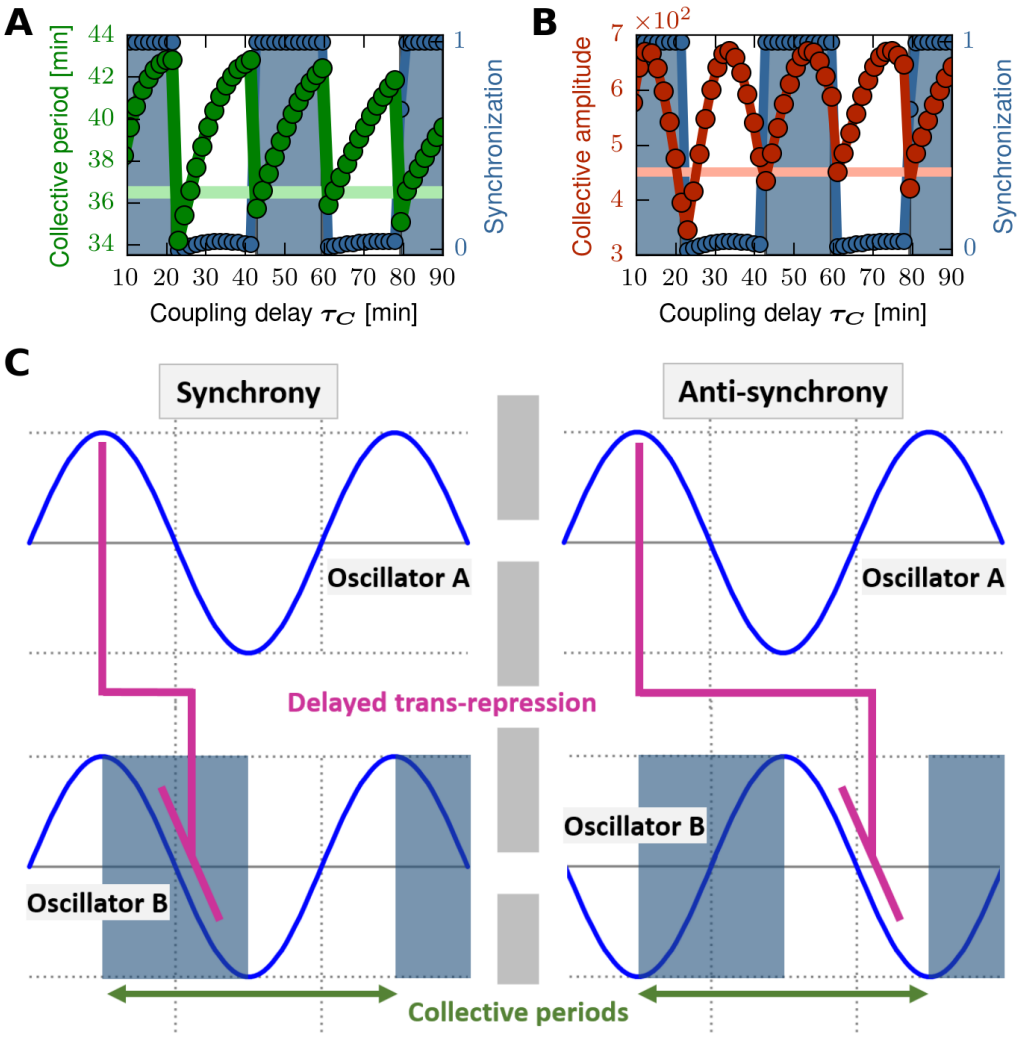

Figure 3.3.: **Collective period, collective amplitude and synchronization of Her1 oscillators critically depend on the coupling delay.** (A, B) Dark blue points represent the synchronization (correlation in expression) between cells calculated by our model. The blue region represents synchronized behaviour predicted by Eq. (3.2). (A) Dark green points represent the collective period and (B) dark red points represent the collective amplitude (B) of Her1 for different coupling delays. As a reference, we plot the autonomous period/amplitude of Her1 (light green/red line); data points correspond to 4×4 cell patches starting in a desynchronized initial condition (Fig. 3.2A). (C) A thought experiment intuitively summarizes the dependence of synchronization and anti-synchronization on the collective period and the coupling delay. The peak of trans-repression lies in the phase of the receiving oscillator where it decreases in amplitude; this determines the synchronization mode if the coupling delay and the collective period are given.

trans-repression of B by A still peaks within the oscillation phase of B with a negative derivative: the two oscillators will anti-synchronize (Fig. 3.3C, right; Lewis, 2003; Tiedemann *et al.*, 2007; Morelli *et al.*, 2009; Herrgen *et al.*, 2010). The condition given by Eq. (3.2) successfully subdivides the phase space in our model (Fig. 3.3A,B, blue regions for synchronization and white regions for anti-synchronization). The estimated coupling delay $\tau_C \approx 50\,\text{min}$ lies in the second region of synchronization (Fig. 3.3A,B), which implies that phase information is not transmitted to the same cycle in the neighbour (Fig. 3.3C, left), but to the consecutive cycle ($k = 1$ in Eq. (3.2)).

In summary, when varying the coupling delay in our model, we observe alternating regions of synchronization and anti-synchronization with a repetitive pattern of collective periods and amplitudes (Fig. 3.3), consistent with a variety of previous theoretical frameworks (Wang *et al.*, 2014; Morelli *et al.*, 2009; Herrgen *et al.*, 2010; Momiji & Monk, 2009). We note that the exchange of phase information between neighbouring PSM cells is skipping one oscillation cycle ($k = 1$ in Eq. (3.2)).

3.4. Time delays control the collective behaviour of cellular oscillators across the PSM

We have shown above that for a given autorepression delay, modulations of the coupling will critically define collective properties of cellular her1 oscillators (Fig. 3.3). We have observed alternating regions of synchronization anti-synchronization with respect to the coupling delay (Fig. 3.3). Evaluating the combined effect of both, the autorepression and the coupling delay, we observe that the regions of synchronization and anti-synchronization gradually shift towards higher coupling delay values when increasing the autorepression delay (Fig. 3.4A). Because the autorepression delay τ_A is included in the coupling delay τ_C (Eq. (2.5)), $\tau_A > \tau_C$ is infeasible (Fig. 3.4A) and possible trajectories in the time delay phase space are restricted: the change in coupling delay must be greater than or equal to the change in the autorepression delay, $\Delta\tau_C \geq \Delta\tau_A$.

Recently, experiments tracking the expression of single cells have revealed that the period of Her1 oscillations increases ~ 1.5-fold from the posterior to the anterior, while the amplitude roughly doubles (Shih *et al.*, 2015). Concordantly with a previous mechanistic model (Ay *et al.*, 2014), we observe that modulated time delays could achieve such variations across the PSM (Fig. 3.4B,C). Moreover, to remain within the second region of synchronization, in which phase information is transmitted to the consecutive cycle in the neighbour ($k = 1$ in Eq. (3.2)), both involved delays must increase as the oscillator travels across the PSM (Fig. 3.4B,C). More precisely, according to our model, it is not sufficient to increase the coupling delay τ_C only by lengthening the autorepression delay τ_A, but an additional DeltaC-dependent time delay change $\Delta\tau_D$ is needed, such that $\Delta\tau_C = \Delta\tau_A + \Delta\tau_D > \Delta\tau_A$. For instance, the delays would change from $\tau_{A,\text{post}} = 10\,\text{min}$ and $\tau_{C,\text{post}} = 50\,\text{min}$ in the posterior to $\tau_{A,\text{ant}} = 20\,\text{min}$ and $\tau_{C,\text{ant}} = 80\,\text{min}$ in the anterior PSM (Fig. 3.4B,C, black arrow); these values are taken as default in the following.

Importantly, we find that the other parameters of the her1 oscillator are not suitable modulators of the collective period. Firstly, the collective period is not sensitive enough with respect to the kinetic rates of synthesis, translation and transcription (Fig. A.2; Ay *et al.*, 2014; Wang *et al.*, 2015). The same is true for the coupling strength, which furthermore affects robustness of synchronization (Figs. A.3 and 3.2A). Lastly, changes in degradation

rates of Her1 protein or mRNA cannot increase both, the collective period and amplitude, simultaneously (Fig. A.2).

Taken together, our model suggests that gradients in the autorepression and coupling delays are critical to increase of the collective period and amplitude as experimentally observed (Shih *et al.*, 2015), while allowing neighbouring cells to remain in a synchronized condition.

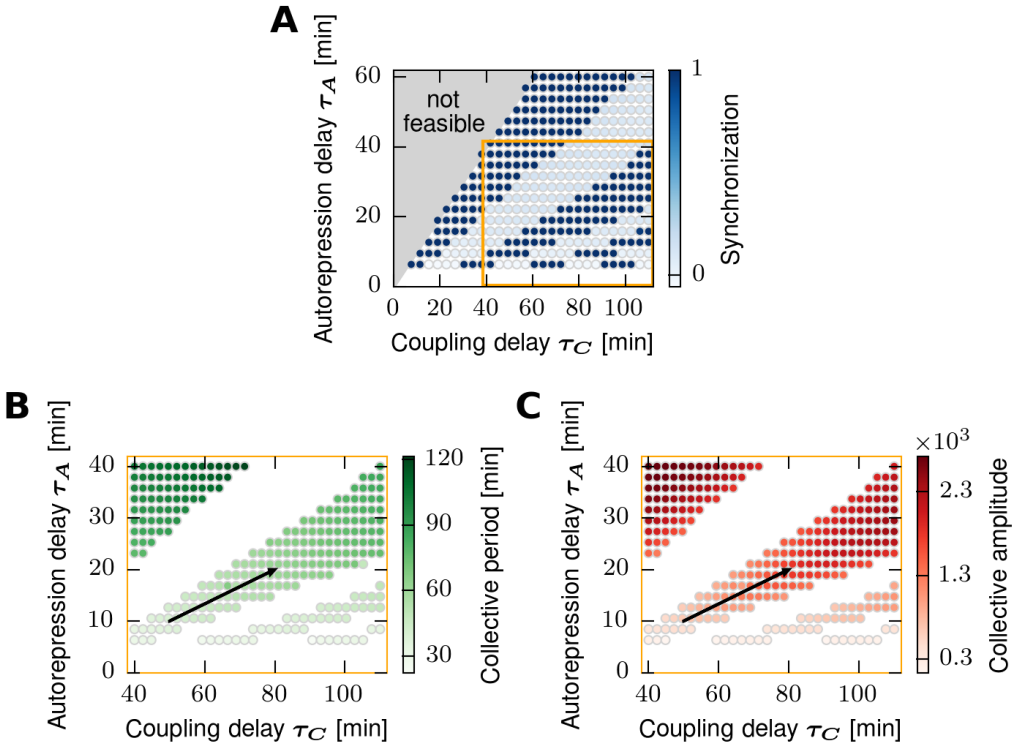

Figure 3.4.: **The time delay phase space of coupled Her1 oscillators reveals a path for synchronized oscillations with increasing collective periods and amplitudes.** (A) Regions of synchronization (dark blue) and anti-synchronization (light blue) observed in the time delay phase space; the coupling delay contains the autorepression delay (Eq. (2.5)), which constrains the phase space (infeasible region coloured in light grey). (B, C) A subspace of (A) is shown (indicated by the orange frames); the anti-synchronized states are hidden (white region); the black arrows represent an exemplary path for cellular oscillator as it moves across the PSM (Fig. 1.1), with increasing collective period (B) and amplitude (C) as indicated from experiments (Shih *et al.*, 2015). All data points correspond to 4×4 cell patches starting in a desynchronized initial condition (Fig. 3.2A).

3.5. Travelling waves in the presence of spatiotemporal time delay gradients

In Notch pathway mutants, the coupling between neighbouring cells is interrupted and the expression of HES/HER oscillates autonomously. In this case, their oscillatory dynamics that

can be regulated on a large scale only by the autorepression delay (Figs. 3.1 and A.4). In contrast, in the wild type, HES/HER oscillatory dynamics arise from a different mechanism (Fig. 3.3): cells attain a locally collective period and amplitude, both of which can be modulated on a large scale only by changing both time delays of the system at the same time (Figs. 3.4 and A.4). In the following, we show that both mechanisms, in the wild type and the mutant, lead to travelling waves, in principle.

First, we simulate the temporal behaviour of a local group of homogeneous cells while increasing the time delays as suggested above (Fig. 3.4A,B, black arrow), which leads to successively longer oscillations with higher amplitude in both scenarios, with autonomous and coupled oscillators (Fig. 3.5A,B). When assuming continuous cell flow, the time a group of cells has spent travelling across the domain is also reflected by their position. It is unknown, whether the dynamics of the cellular oscillators are controlled by positional or temporal information (Oates *et al.*, 2012; Shih *et al.*, 2015). Both interpretations are possible.

We observe that in the case of uncoupled oscillators, initial synchrony is gradually lost (Fig. 3.5A), leading to severe irregularities in the wave pattern (Fig. 3.5C). This corresponds well with experimentally observed posterior segmentation defects in Notch pathway mutants (Jiang *et al.*, 2000).

Our model suggests that in the case of autonomous cells, representing the Notch mutant, only a gradient in the autorepression delay τ_A is needed to control the oscillatory dynamics (Fig. 3.5A) and to form travelling waves. However, for coupled cells, i.e. when Notch signalling is present, changing the autorepression delay, which is also included in the coupling delay τ_C, is not sufficient. Such a case would lead to a switch to a salt-and-pepper patterning regime (Fig. A.5). As we have hypothesized above, an additional DeltaC-dependent time delay change $\Delta\tau_D$ is needed for the emergence of travelling waves (Fig. 3.5D), such that $\Delta\tau_C = \Delta\tau_A + \Delta\tau_D > \Delta\tau_A$.

Taken together, we show that in the absence of cell-cell coupling, a delay in the HES/HER autorepression alone is sufficient to lead to travelling waves of HES/HER expression. In contrast, when the cells are coupled, an additional DeltaC-dependent delay is required in order to maintain the cells synchronized.

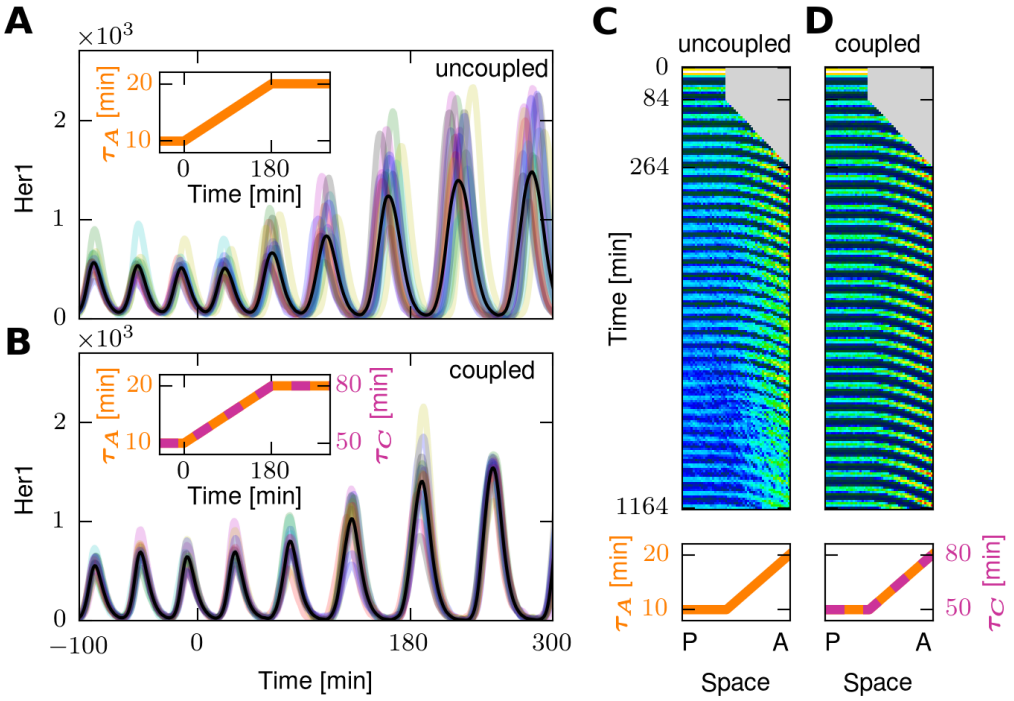

Figure 3.5.: **Travelling waves of autonomous or coupled oscillators.** (A, B) Trajectories of autonomous (A) and coupled Her1 oscillations (B) in a group of 4×4 cells, in the presence of a temporal linear gradient in the autorepression delay τ_A and the coupling delay τ_C between the timepoints 0 min and 180 min (small embedded plots); black lines correspond to the average trajectories. (C, D) Kymographs of travelling wave series formed by autonomous (C) and coupled Her1 oscillators (D) under the influence of time delay gradients (bottom); at every time point (6 min intervals), the 4×50 tissue representing the PSM has been averaged over the medio-lateral axis; after 264 min, a steady cell flow is maintained (for details refer to the Methods section). All time delay gradients correspond to the black arrow in Fig. 3.4B,C. The noise level in the simulations corresponds to the value 10^{-2} in Fig. 3.2B (see Section 2.2 for details).

4. Discussion

4.1. A reduced mechanistic model recapitulates travelling waves in the PSM

Recent cell-based models of somitogenesis have aimed to integrate explicitly the increasing amount of new experimental observations in a mechanistic network (Hester *et al.*, 2011; Tiedemann *et al.*, 2012; Ay *et al.*, 2013). Incidentally, this resulted in increasingly complex models, compared to the first simple autorepression models of the segmentation clock (Lewis, 2003; Monk, 2003). We are convinced that examining minimal models can be an instructive approach to gain a more fundamental understanding of complex processes (Goldenfeld & Kadanoff, 2008). Therefore, we propose a simple model in a reduced form, compared to the model of Julian Lewis (Lewis, 2003; Eqs. (2.1) and (2.2)). Our model includes only one autorepression cycle over her1 and couples neighbouring oscillators via trans-repression (Eqs. (2.3) and (2.4)). A similar model has been used for analytical purposes by Wang *et al.* (2014), but we incorporate only two time delays, instead of three. Because the her7;hes6 double mutant is segmented normally in most cases, we assume that *her1* is sufficient to drive the cellular oscillators in the PSM. In appreciation of Julian Lewis, we show that his simple initial *her1* model is still remarkably powerful (Lewis, 2003; Lander, 2014). It is the key which we use to understand the principles governing the travelling wave that controls the rhythmicity of the vertebrate segmentation. On this foundation, we offer a reduced mechanistic model which recapitulates the properties of travelling waves in the PSM studied over decades in experiments and a variety of theoretical frameworks.

We show that the travelling wave formation in zebrafish can be understood by the control of three parameters: the HES/HER autorepression delay, the intercellular coupling delay, and the coupling strength. These three parameters critically define three emergent local properties: the collective period, the collective amplitude, and the synchronization of neighbouring presomitic cells. As found in a more complex framework (Ay *et al.*, 2014), we observe that a spatiotemporal gradient in the time delays can explain the cellular oscillator dynamics monitored *in vivo* (Fig. 3.4B,C; Shih *et al.*, 2015). Concomitantly, a synchronizing condition is maintained (Fig. 3.4A). There are many related topics which are not addressed by our reduced *her1* model and remain unresolved mechanistically, such as (i) the control of the wavefront and the oscillation arrest (Oates *et al.*, 2012; Shih *et al.*, 2015), (ii) the temperature sensitivity of the somitogenesis period (Schröter *et al.*, 2008), (iii) the scaling of the pattern with the body size (Cooke, 1975; Tam, 1981), and (iv) the scaling observed during *ex vivo* segmentation (Lauschke *et al.*, 2013). Concerning the latter, I discuss theoretical and biological hypotheses separately in Appendix A.3.

4.2. Time delays in autonomous and coupled *her1* oscillators and their spatiotemporal control

We find that the oscillatory dynamics within the travelling wave in the PSM are best understood by examining the trajectory of the PSM cells through their time delay phase space (Fig. 3.4). Firstly, we emphasize the role of the autorepression delay in modulating the period of the autonomous Her1 oscillator (Fig. 3.1). A successive increase of this delay in autonomous oscillators will lead to a period and amplitude profile which is on the same scale as measured experimentally in the wild type (Figs. 3.5A and A.4; Shih *et al.*, 2015). An effective translational delay gradient of Her1 has been measured experimentally (Ay *et al.*, 2014). The desynchronization hypothesis states that uncoupled oscillators will lose their synchrony successively; this synchrony is established earlier in development by simultaneous gene induction of *her1* (Figs. 3.2A and 3.5A,C; Jiang *et al.*, 2000; Riedel-Kruse *et al.*, 2007; Özbudak & Lewis, 2008; Liao & Oates, 2016).

The second time delay in our model, the coupling delay, represents the time needed for coupled oscillators to exchange Her1 oscillation phase information. This delay is not relevant in Notch pathway mutants, where juxtacrine coupling is interrupted and cells oscillate autonomously. We notice that due to the long deltaC expression delay of 40 min, the information exchange in the wild type must be skipping one oscillation cycle ($k = 1$ in Eq. (3.2), second region of synchronization in Figs. 3.3 and 3.4A). In general, the coupling delay is a potent regulator of collective period and amplitude, and defines sharp transitions between synchronization and salt-and-pepper patterning (Figs. 3.2C,D and 3.3; see further discussion below).

Because the coupling delay incorporates the autorepression delay, changes in coupling delay must be greater or equal to the changes in autorepression delay for an individual cell that moves through the time delay phase space (Fig. 3.4A). We have discussed that for autonomous Her1 oscillators it is only possible to modulate the autorepression delay to achieve reasonable period and amplitude gradients (Figs. 3.5A and A.4). This mechanism, however, is not applicable for the coupled Her1 oscillators (Fig. A.5), which modulate their autonomous period additionally by exchanging phase information with their neighbours. For the wild type, our model indicates only one mechanism to achieve gradients in collective period and amplitude, and to remain in the same region of synchronization (Fig. 3.4): besides the autorepression delay gradient, an additional spatiotemporal gradient in the deltaC expression delay is required to form travelling waves (Fig. 3.5D). These predictions are in line with a more complex model proposed by others (Ay *et al.*, 2014). The fact that the DeltaC stripe precedes the Her1 stripe only in the middle of the PSM is an additional indication for differential spatiotemporal modulation of time delays (Jülich *et al.*, 2005).

Our results put the desynchronization hypothesis, that the essential role of Notch signalling in somitogenesis is to maintain synchrony in neighbouring PSM oscillators (Jiang *et al.*, 2000; Riedel-Kruse *et al.*, 2007; Özbudak & Lewis, 2008; Liao & Oates, 2016), into perspective: Notch signalling also regulates the collective dynamics of cellular oscillators in terms of period and amplitude — and thereby shapes the travelling wave pattern.

Whether the oscillatory dynamics across the PSM are controlled by positional or temporal information is an open question (Oates *et al.*, 2012; Shih *et al.*, 2015). The 'gradient by inheritance' model suggests that *fgf8*, and possibly also *wnt3A*, are transcribed only in the tail bud and their mRNA is gradually decaying in the presomitic cells that are left behind

by the proliferating tail bud (Dubrulle & Pourquié, 2004; Aulehla & Pourquié, 2010; Bajard *et al.*, 2014). If one of these two signalling pathways would be involved in the shortening of the autorepression and coupling time delays, this would explain how temporal information of mRNA decay progression is translated into positional information by successive cell flow. In contrast, my current understanding of the *ex vivo* segmentation process, indicates that the oscillatory dynamics are controlled by positional information (see Appendix A.3).

4.3. Unifying hypotheses for the role of time delays in juxtacrine signalling

A wide variety of time-delayed coupling phenomena similar to the one investigated here, are currently studied across the natural sciences (Sadeghi & Valizadeh, 2014; Pavlides *et al.*, 2015; Vanag *et al.*, 2016; Wetzel *et al.*, 2017). Recently, a unifying hypothesis for the time-delayed coupling mediated by Notch in neurogenesis and somitogenesis has been proposed (Shimojo *et al.*, 2016; Shimojo & Kageyama, 2016): a difference in coupling delays between biological tissues could explain why dynamic salt-and-pepper patterning is observed in the developing brain and synchronization is observed in the PSM (Shimojo *et al.*, 2016; Shimojo & Kageyama, 2016). Mice mutants with different gene length, and therefore different transcriptional delays, exhibited oscillation death in the PSM on a tissue level (Shimojo & Kageyama, 2016). Still, to gain a broader understanding, single cell oscillations remain to be tracked under these intriguing new experimental conditions. Based on our model of the zebrafish PSM oscillator, we hypothesize that tissue-level oscillations are damped in coupling delay mutants by the shift to a dynamic salt-and-pepper patterning regime (Figs. 3.2C,D and 3.3). But importantly, the idea that the coupling delay varies between different tissues could apply in an even wider scope: It has been shown that during angiogenesis, upregulation of Dll4 by high Vegf signalling leads to a switch from dynamic salt-and-pepper patterning, required for tip versus stalk fate selection, to pathological synchronization of Dll4-Notch dynamics, leading to vessel expansion (Ubezio *et al.*, 2016). Within our theoretical framework, such a switch would imply that Dll4 upregulation modulates the ratio of the collective period and the coupling delay of the cellular oscillators (illustrated in Fig. 3.3C), driving the system into a region of synchronization (Fig. 3.4A). The sensitivity analysis of the emergent collective period (Figs. 3.4B, A.2 and A.3) suggests that time delays are the most potent regulators — and their modulation could be responsible for such a switch. Time delays might control both, the oscillatory dynamics within the PSM and the varying synchronization behaviour among different tissues. Currently, a biological mechanism explaining how time delays are regulated, is not known.

Altogether, these recent advances in somitogenesis, neurogenesis and angiogenesis support the view that time-delayed coupling of cellular oscillators via juxtacrine Notch signalling is a fundamental principle of developmental biology (Shimojo & Kageyama, 2016). The coupling behaviour controls whether cells differentiate collectively as in the PSM or whether a number of individual cells differentiate, as it is the case during the formation of the cerebral cortex or the branching of blood vessels. Additionally, the cellular oscillators in the PSM, in an intricate way, define the rhythmicity of segmentation via the formation of travelling waves.

5. Conclusion and Outlook

In this thesis, I have studied the theoretical basis of travelling waves occurring in the presomitic mesoderm of developing vertebrates. These waves of gene expression control the rhythm with which pairs of somites sequentially emerge on both sides of the notochord (Oates *et al.*, 2012; Hubaud & Pourquié, 2014). The differentiation of these somites into anatomical modules of vertebrae and muscles, sculptures the body plan of the developing embryo — and it will later define its mode of locomotion (Ward & Mehta, 2011).

The travelling waves emerge from cells with oscillating gene expression. The oscillations are driven by delayed autorepression: a gene represses itself in a negative feedback loop via the protein it encodes for (Palmeirim *et al.*, 1997; Cooke, 1998; Bessho *et al.*, 2003; Lewis, 2003; Monk, 2003). The travelling waves emerge, when the cyclic gene expression of cells is locally synchronized (Jiang *et al.*, 2000; Lewis, 2003; Giudicelli *et al.*, 2007; Liao & Oates, 2016) and a gradient in oscillation period is present (Kærn *et al.*, 2000; Jaeger & Goodwin, 2001; Tiedemann *et al.*, 2007; Uriu *et al.*, 2009; Ay *et al.*, 2014).

Together with Dr. Marcelo Boareto and Dr. Prof. Dagmar Iber, I have aimed to integrate these principles — with the care and rigour — in the simplest form that would allow to discuss the knowledge gathered over decades of scientific research in the field. Our model characterizes, how cells communicate locally via Notch signalling, how they synchronize and how they adapt their behaviour collectively. The oscillatory dynamics of the cyclic components in these cells, shape the travelling wave and are likely to be controlled by time delays (Ay *et al.*, 2014). Our model summarizes these delays in two fundamentally different abstract delays: the delay in the autorepression loop and the delay that transmits phase information to the neighbouring cells.

We hypothesize that the properties controlled by these two time delays not only lead to travelling wave formation in somitogenesis, but also govern neurogenesis (Shimojo *et al.*, 2016; Shimojo & Kageyama, 2016) and angiogenesis. During these two developmental processes, dynamic salt-and-pepper patterning of Delta-Notch expression is observed (Kageyama *et al.*, 2008; Shimojo *et al.*, 2008; Ubezio *et al.*, 2016). Our model suggests that differences in the two time delays that we define, are most likely involved between tissues with different synchronization behaviour of the Notch-Delta dynamics.

With this thesis, I want to contribute to the understanding of somitogenesis as an intricately and beautifully timed and regulated process. This complex machinery is adaptive to varying body size (Cooke, 1975; Tam, 1981) and temperature (Schröter *et al.*, 2008) - a fascinating fact, for which no explanation is currently known. With my last contribution, the theoretical study of the *ex vivo* segmentation, I have gained an insight into the open questions posed by this current mystery. How does the travelling wave pattern scale with the size of the presomitic mesoderm? Is it shaped by temporal or spatial cues? And how does it encode for segmentation events? Once the scientific community sheds more light into these unknown grounds, our reduced mechanistic model could be of value again — to extend it in simple terms and to gain a conceptual understanding of the principles that govern development.

Bibliography

Andersson, E.R., Sandberg, R. and Lendahl, U. (2011). Notch signaling: simplicity in design, versatility in function. Development 138, 3593-3612.

Aulehla, A., Wehrle, C., Brand-Saberi, B., Kemler, R., Gossler, A., Kanzler, B. and Herrmann, B. G. (2003). Wnt3a plays a major role in the segmentation clock controlling somitogenesis. Dev. Cell 4, 395–406.

Aulehla, A., Wiegraebe, W., Baubet, V., Wahl, M. B., Deng, C., Taketo, M., Lewandoski, M. and Pourquié, O. (2008). A β-catenin gradient links the clock and wavefront systems in mouse embryo segmentation. Nat. Cell Biol. 10, 186-193.

Aulehla, A., and Pourquié, O. (2010). Signaling gradients during paraxial mesoderm development. Cold Spring Harb. Perspect. Biol. 2, a000869.

Ay, A., Knierer, S., Sperlea, A., Holland, J. and Özbudak, E. M. (2013). Short-lived Her proteins drive robust synchronized oscillations in the zebrafish segmentation clock. Development 140, 3244-3253.

Ay, A., Holland, J., Sperlea, A., Devakanmalai, G. S., Knierer, S., Sangervasi, S., Stevenson, A. and Özbudak, E. M. (2014). Spatial gradients of protein-level time delays set the pace of the traveling segmentation clock waves. Development 141, 4158-4167.

Bajard, L., Morelli, L. G., Ares, S., Pécréaux, J., Jülicher, F. and Oates, A. C. (2014). Wnt-regulated dynamics of positional information in zebrafish somitogenesis. Development 141, 1381-1391.

Barkai, N. and Shilo, B.-Z. (2013). Developmental biology: Segmentation within scale. Nature 493, 32–34.

Bessho, Y., Hirata, H., Masamizu, Y. and Kageyama, R. (2003). Periodic repression by the bHLH factor Hes7 is an essential mechanism for the somite segmentation clock. Genes Dev. 17, 1451-1456.

Clewley, R. H., Sherwood, W. E., LaMar, M. D. and Guckenheimer, J. M. (2007). PyDSTool, a software environment for dynamical systems modeling. URL http://pydstool.sourceforge.net

Cooke, J. (1975). Control of somite number during morphogenesis of a vertebrate, Xenopus laevis. Nature 254, 196-199.

Cooke, J. (1998). A gene that resuscitates a theory-somitogenesis and a molecular oscillator. Trends Genet. 14, 85-88.

Cooke, J. and Zeeman, E. C. (1976). A clock and wavefront model for control of the number of repeated structures during animal morphogenesis. J. Theor. Biol. 58, 455-476.

del Alamo, D., Rouault, H. and Schweisguth, F. (2011). Mechanism and significance of cis-inhibition in Notch signalling. Curr. Biol. 21, R40-47.

Delaune, E. A., François, P., Shih, N. P. and Amacher, S. L. (2012). Single-cell-resolution imaging of the impact of Notch signaling and mitosis on segmentation clock dynamics. Dev. Cell 23, 995-1005.

Dequeant, M. L., Glynn, E., Gaudenz, K., Wahl, M., Chen, J., Mushegian, A. and Pourquié O. (2006). A complex oscillating network of signaling genes underlies the mouse segmentation clock. Science 314, 1595-1598.

Diez del Corral, R., Olivera-Martinez, I., Goriely, A., Gale, E., Maden, M. and Storey, K. (2003). Opposing FGF and retinoid pathways control ventral neural pattern, neuronal differentiation, and segmentation during body axis extension. Neuron 40:65-79.

Dubrulle, J., McGrew, M. J. and Pourquié, O. (2001). FGF signaling controls somite boundary position and regulates segmentation clock control of spatiotemporal Hox gene activation. Cell 106, 219-232.

Dubrulle, J. and Pourquié, O. (2004). fgf8 mRNA decay establishes a gradient that couples axial elongation to patterning in the vertebrate embryo. Nature 427, 419-422.

Dunty, W.C. Jr., Biris, K. K., Chalamalasetty, R. B., Taketo, M. M., Lewandoski, M. and Yamaguchi, T. P. (2008). Wnt3a/*beta*-catenin signaling controls posterior body development by coordinating mesoderm formation and segmentation. Development 135, 85-94.

Flunkert, V. and Schoell, E. (2009). Pydelay - a python tool for solving delay differential equations. arXiv:0911.1633.

Giudicelli, F., Özbudak, E. M., Wright, G. J. and Lewis, J. (2007). Setting the tempo in development: an investigation of the zebrafish somite clock mechanism. PLoS Biol. 5, e150.

Goldbeter, A., Gonze, D. and Pourquié, O. (2007). Sharp developmental thresholds defined through bistability by antagonistic gradients of retinoic acid and FGF signaling. Dev. Dyn. 236, 1495-1508.

Goldenfeld, N. and Kadanoff, L. (1999). Simple Lessons from Complexity. Science 284, 87

Goldshmit, Y., Sztal, T. E., Jusuf, P. R., Hall, T. E., Nguyen-Chi, M. and Currie, P. D. (2012). Fgf-Dependent Glial Cell Bridges Facilitate Spinal Cord Regeneration in Zebrafish. J. Neurosci. 32, 7477–92.

Götz, M. and Huttner, W.B. (2005). The cell biology of neurogenesis. Nat. Rev. Mol. Cell Biol. 6, 777-788.

Griffith, J. S. (1968). Mathematics of cellular control processes. I. Negative feedback to one gene. II. Positive feedback to one gene. J. Theor. Biol. 20, 202–216.

Hanisch, A., Holder, M. V., Choorapoikayil, S., Gajewski, M., Özbudak, E. M. and Lewis J. (2013). The elongation rate of RNA polymerase II in zebrafish and its significance in the somite segmentation clock. Development 140, 444-453.

Harima, Y., Takashima, Y., Ueda, Y., Ohtsuka, T. and Kageyama, R. (2013) Accelerating the tempo of the segmentation clock by reducing the number of introns in the Hes7 gene. Cell Rep. 3, 1-7.

Henry, C. A., Urban, M. K., Dill, K. K., Merlie, J. P., Page, M. F., Kimmel, C. B. and Amacher, S. L. (2002). Two linked hairy/Enhancer of split-related zebrafish genes, her1 and her7, function together to refine alternating somite boundaries. Development 129, 3693-3704.

Hermanns, T., Thombansen, U., Nießen, M., Jansen, U., and Schulz, W. (2016). Modeling for Self-Optimization in Laser Cutting. In F. Miranda and C. Abreu (Eds.), Handbook of Research on Computational Simulation and Modeling in Engineering (pp. 586-617). Hershey, PA: IGI Global.

Herrgen, L., Ares, S., Morelli, L. G., Schröter, C., Jülicher, F. and Oates, A. C. (2010). Intercellular coupling regulates the period of the segmentation clock. Curr. Biol. 20, 1244-53.

Hester, S. D., Belmonte, J. M., Gens, J. S., Clendenon, S.G. and Glazier, J. A. (2011). A multi-cell, multi-scale model of vertebrate segmentation and somite formation. PLoS Comput Biol. 7, e1002155.

Hirata, H., Yoshiura, S., Ohtsuka, T., Bessho, Y., Harada, T., Yoshikawa, K. and Kageyama R. (2002). Oscillatory expression of the bHLH factor Hes1 regulated by a negative feedback loop. Science 298, 840-843.

Holley, S. A., Jülich, D., Rauch, G. J., Geisler, R. and Nüsslein-Volhard C. (2002). her1 and the notch pathway function within the oscillator mechanism that regulates zebrafish somitogenesis. Development 129, 1175-1183.

Hori, Y., Takada, M. and Hara, S. (2013). Biochemical oscillations in delayed negative cyclic feedback: Existence and profiles. Automatica 9, 2581-2591.

Horikawa, K., Ishimatsu, K., Yoshimoto, E., Kondo, S. and Takeda, H. (2006). Noise-resistant and synchronized oscillation of the segmentation clock. Nature 441, 719-723.

Hoyle, N. P. and Ish-Horowicz, D. (2013). Transcript processing and export kinetics are rate-limiting steps in expressing vertebrate segmentation clock genes. Proc. Natl. Acad. Sci. USA 110, E4316-E432.

Hubaud, A. and Pourquié, O. (2014). Signalling dynamics in vertebrate segmentation. Nat. Rev. Mol. Cell Biol. 15, 709-21.

Jaeger, J. and Goodwin, B. C. (2001). A cellular oscillator model for periodic pattern formation. J. Theor. Biol. 213, 171-181.

Jiang, Y.-J., Aerne, B. L., Smithers, L., Haddon, C., Ish-Horowicz, D. and Lewis, J. (2000). Notch signalling and the synchronization of the somite segmentation clock. Nature 408, 475-479.

Jenkins, R. P., Hanisch, A., Soza-Ried, C., Sahai, E. and Lewis, J. (2015). Stochastic Regulation of her1/7 Gene Expression Is the Source of Noise in the Zebrafish Somite Clock Counteracted by Notch Signalling. PLoS Comput. Biol., 11.

Jörg, D. J., Morelli, L. G., Soroldoni, D., Oates, A. C. and Jülicher, F. (2015). Continuum theory of gene expression waves during vertebrate segmentation. New J. Phys. 17, 093042.

Jörg, D. J., Oates, A. C. and Jülicher, F. (2016). Sequential pattern formation governed by signaling gradients. Phys. Biol. 13, 05LT03.

Jülich, D., Hwee Lim, C., Round, J., Nicolaije, C., Schroeder, J., Davies, A., Geisler, R., Lewis, J., Jiang, Y.-J. and Holley, S. A. (2005). beamter/deltaC and the role of Notch ligands in the zebrafish somite segmentation, hindbrain neurogenesis and hypochord differentiation. Dev. Biol. 286, 391-404.

Kærn, M., Menzinger, M. and Hunding, A. (2000). Segmentation and Somitogenesis derived from phase dynamics in growing oscillatory media. J. Theor. Biol. 207, 473-493.

Kageyama, R., Ohtsuka, T., Shimojo, H. and Imayoshi, I. (2008). Dynamic Notch signaling in neural progenitor cells and a revised view of lateral inhibition. Nature neuroscience 11, 1247-1251.

Kawamura, A., Koshida, S., Hijikata, H., Sakaguchi, T., Kondoh, H. and Takada, S. (2005). Zebrafish hairy/enhancer of split protein links FGF signaling to cyclic gene expression in the periodic segmentation of somites. Genes Dev. 19, 1156 -1161.

Kim, J., Shin, D., Jung, S., Heslop-Harrison, P. and Cho, K. (2010). A design principle underlying the synchronization of oscillations in cellular systems. J. Cell Sci. 123, 1537-1543.

Kim, W., Matsui, T., Yamao, M., Ishibashi, M., Tamada, K., Takumi, T., Kohno, K., Oba, S., Ishii, S., Sakumura, Y. et al. (2011). The period of the somite segmentation clock is sensitive to Notch activity. Mol. Biol. Cell 22, 3541-3549.

Krol, A., Roellig, D., Dequeant, M. L., Tassy, O., Glynn, E., Hattem, G., Mushegian, A., Oates, A. C. and Pourquié, O. (2011). Evolutionary plasticity of segmentation clock networks. Development 138, 2783-2792.

Lander, A. D. (2014). Making sense in biology: an appreciation of Julian Lewis. BMC Biol. 12, 57.

Lauschke, V. M., Tsiairis, C. D., François, P. and Aulehla, A. (2013). Scaling of embryonic patterning based on phase-gradient encoding. Nature 493, 101-105.

Lewis, J. (2003). Autoinhibition with transcriptional delay: a simple mechanism for the zebrafish somitogenesis. oscillator. Curr. Biol. 13, 1398-1408.

Liao, B. K., Jörg, D. J. and Oates, A. C. (2016). Faster embryonic segmentation through elevated Delta-Notch signalling. Nat. Commun. 11861.

Liao, B. K. and Oates, A. C. (2016). Delta-Notch signalling in segmentation. Arthropod. Struct. Dev. [Epub ahead of print]. doi: 10.1016/j.asd.2016.11.007.

Mara, A., Schroeder, J., Chalouni, C. and Holley, S. A. (2007). Priming, initiation and synchronization of the segmentation clock by deltaD and deltaC. Nat. Cell Biol. 9, 523-530.

Maroto, M., Dale, J. K., Dequéant, M. L., Petit, A. C. and Pourquié O. (2005). Synchronised cycling gene oscillations in presomitic mesoderm cells require cell-cell contact. Int. J. Dev. Biol. 49, 309-315.

Masamizu, Y., Ohtsuka, T., Takashima, Y., Nagahara, H., Takenaka, Y., Yoshikawa, K., Okamura, H. and Kageyama, R. (2006). Real-time imaging of the somite segmentation clock: revelation of unstable oscillators in the individual presomitic mesoderm cells. Proc. Natl. Acad. Sci. USA 103, 1313-1318.

Matsuda, M. and Chitnis A. B. (2009). Interaction with Notch determines endocytosis of specific Delta ligands in zebrafish neural tissue. Development 136, 197-206.

Momiji, H. and Monk, N. A. (2009). Oscillatory Notch-pathway activity in a delay model of neuronal differentiation. Phys. Rev. E Stat. Nonlin. Soft Matter Phys. 80, 021930.

Monk, N. A. (2003). Oscillatory expression of Hes1, p53, and NF-κB driven by transcriptional time delays. Curr. Biol. 13, 1409-13.

Morelli, L. G., Ares, S., Herrgen, L., Schröter, C., Jülicher, F. and Oates A. C. (2009). Delayed coupling theory of vertebrate segmentation. HFSP J. 3, 55-66.

Naiche, L. A., Holder, N. and Lewandoski, M. (2011). FGF4 and FGF8 comprise the wavefront activity that controls somitogenesis. Proc. Natl. Acad. Sci. USA 108, 4018-4023.

Niebur, E., Schuster, H. G. and Kammen, D. M. (1991). Collective frequencies and metastability in networks of limit-cycle oscillators with time delay. Phys. Rev. Lett. 67, 2753-2756.

Niederreither, K., McCaffery, P., Dräger, U. C., Chambon, P. and Dollé, P. (1997). Restricted expression and retinoic acid-induced downregulation of the retinaldehyde dehydrogenase type 2 (RALDH-2) gene during mouse development. Mech. Dev. 62, 67-78.

Novak, B. and Tyson, J. J. (2008). Design principles of biochemical oscillators. Nat. Rev. Mol. Cell Biol. 9, 981-991.

Oates, A. C. and Ho, R. K. (2002). Hairy/E(spl)-related (Her) genes are central components of the segmentation oscillator and display redundancy with the Delta/Notch signaling pathway in the formation of anterior segmental boundaries in the zebrafish. Development 129, 2929-2946.

Oates, A. C., Morelli, L. G. and Ares, S. (2012). Patterning embryos with oscillations: structure, function and dynamics of the vertebrate segmentation clock. Development 139, 625-39.

Oginuma, M., Niwa, Y., Chapman, D. L. and Saga, Y. (2008). Mesp2 and Tbx6 cooperatively create periodic patterns coupled with the clock machinery during mouse somitogenesis. Development 135, 2555-2562.

Okubo Y et al. Lfng regulates the synchronized oscillation of the mouse segmentation clock via trans-repression of Notch signalling. Nature Commun. 3, 1141 (2012).

Özbudak, E. M. and Lewis, J. (2008). Notch signalling synchronizes the zebrafish segmentation clock but is not needed to create somite boundaries. PLoS Genet. 4, e15.

Palmeirim, I., Henrique, D., Ish-Horowicz, D. and Pourquié, O. (1997). Avian hairy gene expression identifies a molecular clock linked to vertebrate segmentation and somitogenesis. Cell 91, 639-648.

Pavlides, A., Hogan, S. J. and Bogacz, R. (2015). Computational Models Describing Possible Mechanisms for Generation of Excessive Beta Oscillations in Parkinson's Disease. PLoS Comput. Biol. 11, e1004609.

Pikovsky , A., Rosenblum, M. and Kurths, J. (2001). Synchronization: A Universal Concept in Nonlinear Sciences. Cambridge U. Press, New York. ISBN 0-521-59285-2.

Riedel-Kruse I. H., Müller, C. and Oates A. C. (2007). Synchrony dynamics during initiation, failure, and rescue of the segmentation clock. Science 317, 1911-5.

Sadeghi, S. and Valizadeh, A. (2014). Synchronization of delayed coupled neurons in presence of inhomogeneity. Journal of computational neuroscience 36, 55-66.

Saga, Y. (2012). The mechanism of somite formation in mice. Curr. Opin. Genet. Dev. 22, 331-8.

Saga, Y., Hata, N., Koseki, H. and Taketo, M. M. (1997). Mesp2: a novel mouse gene expressed in the presegmented mesoderm and essential for segmentation initiation. Genes Dev. 11, 1827-1839.

Sawada, A., Fritz, A., Jiang, Y.-J., Yamamoto, A., Yamasu, K., Kuroiwa, A., Saga, Y. and Takeda, H. (2000). Zebrafish Mesp family genes, mesp-a and mesp-b are segmentally expressed in the presomitic mesoderm, and Mesp-b confers the anterior identity to the developing somites. Development 127, 1691-1702.

Sawada, A., Shinya, M., Jiang, Y.-J., Kawakami, A., Kuroiwa, A. and Takeda, H. (2001). Fgf/MAPK signalling is a crucial positional cue in somite boundary formation. Development 128, 4873-4880.

Schröter, C., Herrgen, L., Cardona, A., Brouhard, G. J., Feldman, B. and Oates A. C. (2008). Dynamics of zebrafish somitogenesis. Dev. Dyn. 237, 545-553.

Schröter, C., Ares, S., Morelli, L. G., Isakova, A., Hens, K., Soroldoni, D., Gajewski, M., Jülicher, F., Maerkl, S. J., Deplancke, B. et al. (2012). Topology and dynamics of the zebrafish segmentation clock core circuit. PLoS Biol. 10, e1001364.

Shih, N. P., François, P., Delaune, E. A. and Amacher, S. L. (2015). Dynamics of the slowing segmentation clock reveal alternating two-segment periodicity. Development 142, 1785-1793.

Shimojo, H., Isomura, A., Ohtsuka, T., Kori, H., Miyachi, H. and R. Kageyama. (2016). Oscillatory control of Delta-like1 in cell interactions regulate dynamic gene expression and tissue morphogenesis. Genes Dev. 30, 102-116.

Shimojo, H. and Kageyama, R. (2016). Oscillatory control of Delta-like1 in somitogenesis and neurogenesis: a unified model for different oscillatory dynamics. Semin. Cell Dev. Biol. 49, 76-82.

Shimojo, H., Ohtsuka, T. and Kageyama, R. (2008). Oscillations in notch signaling regulate maintenance of neural progenitors. Neuron 58, 52-64.

Soroldoni, D., Jörg, D. J., Morelli, L. G., Richmond, D. L., Schindelin, J., Jülicher, F. and Oates, A. C. (2014). A Doppler effect in embryonic pattern formation. Science 345, 222-5.

Soza-Ried, C., Öztürk, E., Ish-Horowicz, D. and Lewis, J. (2014). Pulses of Notch activation synchronise oscillating somite cells and entrain the zebrafish segmentation clock. Development 141, 1780-1788.

Spence, R., Gerlach, G., Lawrence, C. and Smith, C. (2007). The behaviour and ecology of the zebrafish, Danio rerio. Biol. Rev. Camb. Philos. So. 83, 13–34.

Takahashi, Y., Koizumi, K., Takagi, A., Kitajima, S., Inoue, T., Koseki, H. and Saga, Y. (2000). Mesp2 initiates somite segmentation through the Notch signalling pathway. Nature Genet. 25, 390-396.

Takashima, Y., Ohtsuka, T., González, A., Miyachi, H. and Kageyama, R. (2011). Intronic delay is essential for oscillatory expression in the segmentation clock. Proc. Natl. Acad. Sci. USA 108, 3300-3305.

Tam, P. P. (1981). The control of somitogenesis in mouse embryos. J. Embryol. Exp. Morphol. 65, 103-128.

Tiedemann, H. B., Schneltzer, E., Zeiser, S., Rubio-Aliaga, I., Wurst, W., Beckers, J., Przemeck, G. K. and Hrabé de Angelis, M. (2007). Cell-based simulation of dynamic expression patterns in the presomitic mesoderm. J. Theor. Biol. 248, 120-129.

Tiedemann, H. B., Schneltzer, E., Zeiser, S., Hoesel, B., Beckers, J., Przemeck, G. K. and Hrabé de Angelis, M. (2012) From dynamic expression patterns to boundary formation in the presomitic mesoderm. PLoS Comput. Biol. 8, e1002586.

Rost, F., Eugster, C., Schröter, C., Oates, A. C. and Brusch, L. (2014). Chevron formation of the zebrafish muscle segments. J. Exp. Biol. 217, 3870-3882.

Ubezio, B., Blanco, R. A., Geudens, I., Stanchi, F., Mathivet, T., Jones, M. L., Ragab, A., Bentley, K. and Gerhardt H. (2016). Synchronization of endothelial Dll4-Notch dynamics switch blood vessels from branching to expansion. eLife 5, e12167.

Uriu, K., Morishita, Y. and Iwasa, Y. (2009). Traveling wave formation in vertebrate segmentation. J. Theor. Biol. 257, 385-396.

Vanag, V. K., Smelov, P. S. and Klinshov, V. V. (2016). Dynamical regimes of four almost identical chemical oscillators coupled via pulse inhibitory coupling with time delay. Phys. Chem. Chem. Phys. 18, 5509-20.

Vollmer, J., Fried, P., Aguilar-Hidalgo, D., Sánchez-Aragón, M., Iannini, A., Casares, F. and Iber, D. (2017). Growth control in the Drosophila eye disc by the cytokine Unpaired. Development 144, 837-843.

Wang, Y. Q., Hori, Y., Hara, S. and Doyle, F. J. (2014). Intercellular delay regulates the collective period of repressively coupled gene regulatory oscillator networks. IEEE Trans. Autom. Control 59, 211-216.

Wang, Y. Q., Hori, Y., Hara, S. and Doyle, F. J. (2015). Collective oscillation period of inter-coupled biological negative cyclic feedback oscillators. IEEE Trans. Autom. Control 60, 1392-1397.

Wanglar, C., Takahashi, J., Yabe, T. and Takada, S. (2014). Tbx protein level critical for clock-mediated somite positioning is regulated through interaction between Tbx and Ripply. PLoS ONE 9, e107928.

Ward, A. B. and Mehta, R. S. (2011). Axial elongation in fishes: using morphological approaches to elucidate developmental mechanisms in studying body shape. Integr. Comp. Biol. 50, 1106-1119.

Webb, A. B., Lengyel, I. M., Jörg, D. J., Valentin, G., Jülicher, F., Morelli, L. G., and Oates, A. C. (2016). Persistence, period and precision of autonomous cellular oscillators from the zebrafish segmentation clock. eLife 5, e08438.

Wetzel, L., Jörg, D. J., Pollakis, A., Rave, W., Fettweis, G. and Jülicher, F. (2017). Self-organized synchronization of digital phase-locked loops with delayed coupling in theory and experiment. PLoS ONE 12, e0171590.

Wright, G. J., Giudicelli, F., Soza-Ried, C., Hanisch, A., Ariza-McNaughton, L. and Lewis, J. (2011). DeltaC and DeltaD interact as Notch ligands in the zebrafish segmentation clock. Development 138, 2947-2956.

Yabe, T. and Takada, S. (2016). Molecular mechanism for cyclic generation of somites: lessons from mice and zebrafish. Dev. Growth Differ. 58, 31-42.

Yasuhiko, Y., Haraguchi, S., Kitajima, S., Takahashi, Y., Kanno, J. and Saga, Y. (2006). Tbx6-mediated Notch signaling controls somite-specific Mesp2 expression. Proc. Natl. Acad. Sci. USA 103, 3651-3656.

A. Appendices

A.1. Supplementary figures for the reduced *her1* model

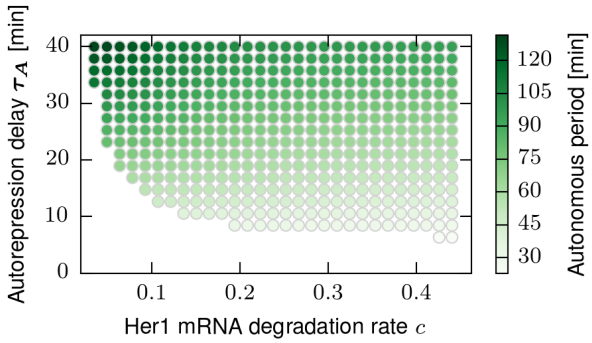

Figure A.1.: **Modulation of the autonomous period of Her1 oscillators**. The autonomous period of Her1 is controlled by the autorepression delay and the degradation rates of the mRNA c (shown) and the protein b (equivalent to c). All data points correspond to 4×4 cell patches.

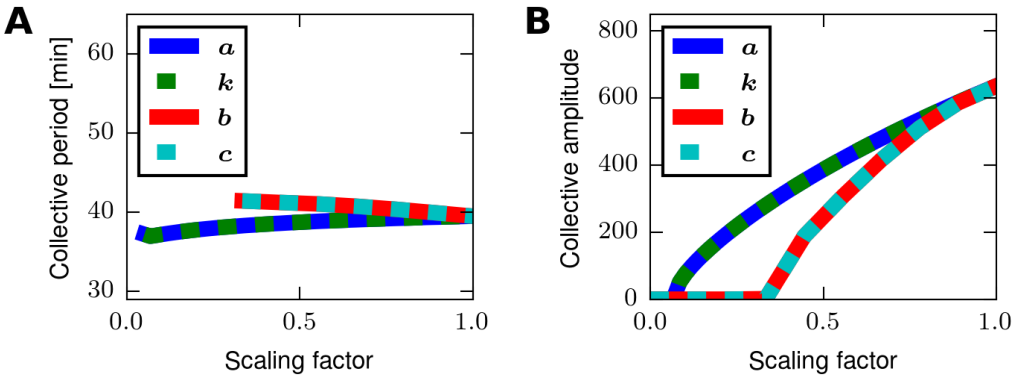

Figure A.2.: **Sensitivity analysis of the kinetic rates associated with the Her1 oscillator in terms of collective period and amplitude**. The effect of kinetic rates in Eqs. (2.3) and (2.4) on the collective period (A) and amplitude (B). Note, that the default values (scaling factor 1) are maximal estimates (Lewis, 2003). All data points correspond to 4×4 cell patches starting in a desynchronized initial condition (Fig. 3.2A).

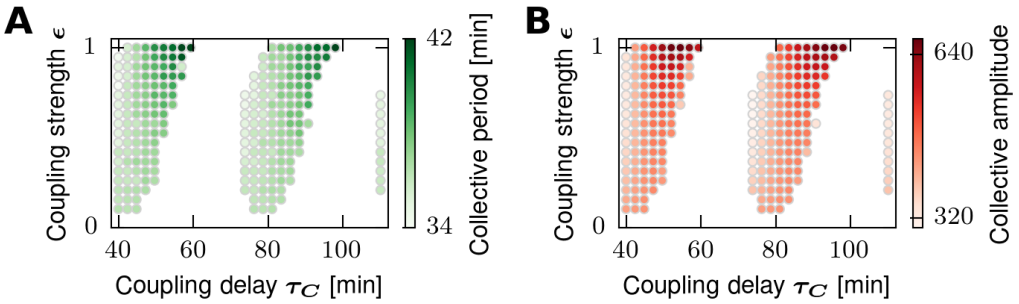

Figure A.3.: **The role of the coupling strength**. The collective periods (A) and amplitudes (B) of Her1 vary more with stronger coupling. The anti-synchronized states are hidden. The synchronized regions are moderately shifted with varying coupling strength. All data points correspond to 4×4 cell patches starting in a desynchronized initial condition (Fig. 3.2A).

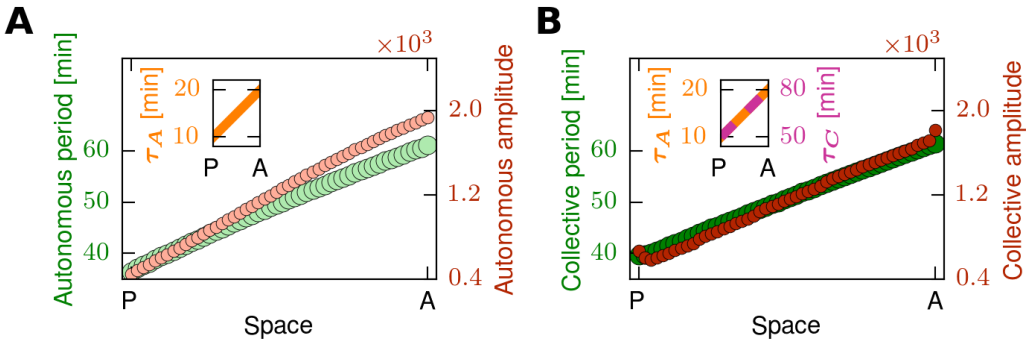

Figure A.4.: **Spatial time delay gradients on a static domain**. (A, B) Collective period and amplitude profiles of Her1 for static and cylindric 4×50 cell tissues with a default linear gradients in the autorepression delay τ_A and the coupling delay τ_C (embedded small plots) along the longer axis (posterior-anterior, P-A); recorded for autonomous (A) and coupled Her1 oscillators (B). In Fig. 3.4, we have used 4×4 cell patches with homogeneous parameter values to approximate the PSM locally, similarly to the approach of others (Tiedemann *et al.*, 2007; Ay *et al.*, 2013). We have concluded that a spatiotemporal gradient in time delays (Fig. 3.4B,C, black arrow) could explain the oscillatory dynamics of recorded across the PSM (Shih *et al.*, 2015). Indeed, when imposing such a gradient spatially, we observe resultant linear gradients of collective period and amplitude of Her1, in space (A, B). For the exemplary gradient, the period and amplitude pattern that we record in the autonomous (A) and the coupled scenario (B) are similar and roughly approximate the single cell wild-type data measured in the PSM by others (Shih *et al.*, 2015).

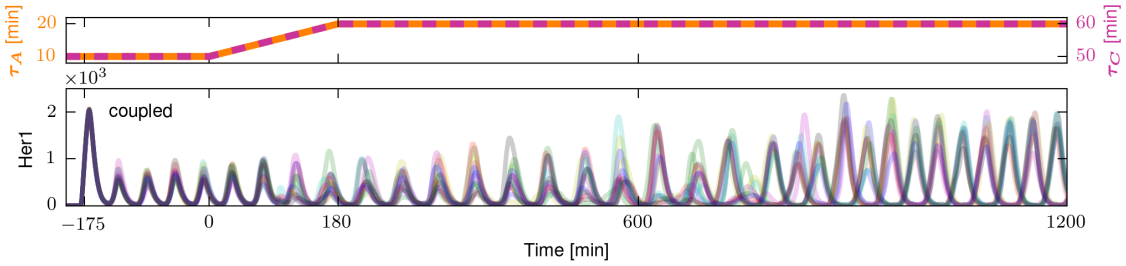

Figure A.5.: **An autorepression delay gradient is not sufficient for travelling wave emergence in the wild type**. Simulation of coupling behaviour in presence of a temporal gradient in the autorepression delay τ_A, which is included in the coupling delay τ_C. Trajectories of coupled Her1 oscillations (bottom) in a group of 4×4cells, in the presence of a temporal linear gradient in time delays between the timepoints 0 min and 180 min (top). The noise level corresponds to the value 10^{-2} in Fig. 3.2B.

A.2. Modelling biological autorepression oscillators

Time-delayed autorepression can be modelled by two different approaches (Novak & Tyson, 2008). The first approach is based on four intermediate components that could represent the shuttling of the mRNA and the protein across the nuclear membrane (Novak & Tyson, 2008). The protein represses the transcription of its gene in the nucleus and the mRNA is translated in the cytosol. The second approach uses delay equations such that the mRNA expression at time t is repressed by the protein abundance at time $t_0 = t - t_i$, where t_i is the time required for mRNA processing and nuclear export as suggested for the PSM oscillator (Lewis, 2003; Takashima *et al.*, 2011; Hoyle & Ish-Horowicz, 2013). In both cases, repression is modelled by a negative Hill function, which is given as

$$H^-(x, x_0, n) = \frac{1}{1 + (\frac{x}{x_0})^n} \tag{A.1}$$

where x is the protein level, x_0 the Hill constant, and n the Hill coefficient.

We have analysed both approaches and we have found that for a shuttling-based oscillator, an unphysiologically high Hill coefficient of roughly $n = 8$ is needed to allow oscillations. This result has been known already (Griffith, 1968). The Hill coefficient represents the cooperativity of the repressing protein. Hes/Her proteins form dimers, implying that an Hill coefficient $n \approx 2$ is expected (Lewis, 2003; Schröter *et al.*, 2012). A lower Hill coefficient can be used by introducing non-linear terms into the differential equations (Novak & Tyson, 2008).

We have decided to use the delay equations in our model of the PSM oscillator due to multiple reasons. First, we do not need additional non-linear terms or high Hill coefficients, as in the case of the shuttling-based oscillator described above. Secondly, we can base our model on the parameters which Julian Lewis estimated for the zebrafish PSM oscillator (Lewis, 2003). The zebrafish oscillator appears to be more reduced than, for instance, the one of mice (Krol *et al.*, 2011), which suits our purposes of addressing conceptual questions.

Most importantly, I think that explicit time delays are more realistic than series of kinetic rates. With explicit time delays, every elementary event is delayed. Which is reasonable,

when considering that mRNAs and proteins change their subcellular location in the process of gene expression and protein secretion. Also, molecular machines, such as polymerases, spliceosomes or ribosomes, have a certain maximal pace at which they process information (Lewis, 2003). These processes are delayed in the order of tens of minutes in the zebrafish PSM (Lewis, 2003; Hanisch *et al.*, 2013; Giudicelli *et al.*, 2007). Using a series of slow kinetic rates, it would be possible, although unlikely, that a gene is instantly transcribed and the corresponding membrane protein molecule occurs at the cell surface in a few time iterations, already — which is physically impossible.

A.3. *Ex vivo* scaling of the oscillation phase gradient

Scaling is a universal biological phenomenon: structures and patterns form proportionally to a reference size, such as the body size or the size of the patterned domain. This phenomenon is still not understood, with intriguing open questions such as (Barkai & Shilo, 2013; Vollmer *et al.*, 2017): How is tissue size measured? How is growth of developing structures terminated in various systems?

In the context of somitogenesis, Lauschke *et al.* (2013) recently introduced an *ex vivo* system, in which scaling of a travelling wave pattern is observed in time during shrinkage of the patterned domain. The scaling of this pattern, i.e. the scaling of the phase gradient in the underlying oscillators, is suggested to directly control the scaling of the segments that are formed during somitogenesis. New questions arise from these observations (Barkai & Shilo, 2013): Could this mechanism also compensate for size variation within a population of individuals? How does the wave pattern encode the formation of the next segment? What is the biological basis for the scaled phase gradient?

Lauschke *et al.* (2013) explanted a monolayer of presomitc mesoderm tissue (mPSM) from the tail bud in mice and monitored a reporter of Lunatic fringe. Lunatic fringe is involved in Notch signalling and is a component of the mice PSM oscillator (Lauschke *et al.*, 2013). In their setup, concentric travelling waves sweep from the center to the periphery of the mPSM (Lauschke *et al.*, 2013). The tissue grows for approximately 20 hours, until segments start to form sequentially from the periphery towards the center (Lauschke *et al.*, 2013). Similar to the *in vivo* case, segmentation coincides with oscillation arrest and expression of *Mesp2* (Lauschke *et al.*, 2013).

Interestingly, Lauschke *et al.* (2013) report that while the process proceeds, the segment width scales with the gradually shorted length (radius) of the remaining mPSM tissue. But not only does the segment width scale - also the wave pattern does: the phase gradient from the center to the outer boundary of the mPSM becomes gradually steeper, such that the time of flight of each kinetic wave remains constant (Lauschke *et al.*, 2013). Moreover, the phase difference between the center at the periphery remains constant at 2π throughout the entire recorded process (Lauschke *et al.*, 2013).

I assume that during the *ex vivo* segmentation described above, the proliferation of the tissue is neglectable. This is not rigorously validated in the paper of (Lauschke *et al.*, 2013), but in the supplementary movies, there is certainly no cell flow visible, as it is *in vivo*. When this assumption holds, this experimental setup becomes very interesting to study: the travelling wave becomes purely kinematic, without any underlying mass transport. In contrast, *in vivo*,

cell flow renders it very challenging to relate spatial oscillation patterns to the oscillation dynamics of individual oscillators (Soroldoni *et al.*, 2014; Jörg *et al.*, 2015).

Interestingly, during my study of the reduced *her1* oscillator, I have noticed the following: the wavelength of the waves, which travel across a static domain with oscillators of linearly increasing oscillation period, decreases in time (Fig. A.6). Therefore, if this domain would shrink artificially to the right extent, representing the segmentation process *ex vivo*, the travelling wave pattern could be scaled in time. Marcelo Boareto introduced me to an interesting phenomenon that I noticed is analogous to this pattern that I observe in our *her1* model: Pendulum waves occur in an array of pendulums with an increasing pendulum length, i.e. an increasing oscillation period. These pendulum waves also decrease in wavelength in time (until the wavelength is so short that strange patterns arise).

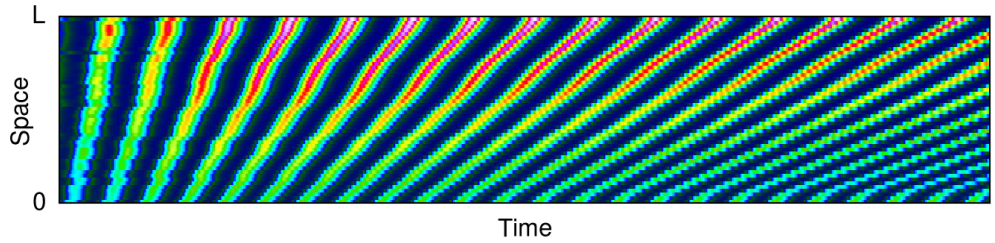

Figure A.6.: **The wavelength of Her1 travelling waves decreases in time on a static domain.** The simulation setup is identical to Fig. A.4B. The collective oscillation period and amplitude are increasing from 0 to L. The plot is a kymograph, where the 4×50 tissue has been averaged over the medio-lateral axis for each time point.

Lauschke *et al.* (2013) have not measured the spatial variation of periods and amplitudes across the mPSM. But considering (i) the visual intensity (i.e. amplitude) distribution in their kymographs, (ii) our knowledge, that travelling waves form in presence of an gradient in oscillation period (Kærn *et al.*, 2000; Jaeger & Goodwin, 2001; Tiedemann *et al.*, 2007; Uriu *et al.*, 2009; Ay *et al.*, 2014), and (iii) the resemblance of Fig. A.6 with the kymographs of Lauschke *et al.* (2013), I have decided to model the *ex vivo* mPSM as an array of sine-based oscillators with increasing periods $T(x)$ and amplitudes. For such an array, I plot a kymograph (Fig. A.7A) by sampling the signal S for time points t_i and locations $x_i \in [0, L]$:

$$S(t_i, x_i) = (x_i + 1)\sin(\frac{2\pi t_i}{T(x_i)}) + x_i + 1 \tag{A.2}$$

Having this complete kymograph, I initiate a segmentation event each time a wave reaches the boundary of the 'mPSM' (Fig. A.7A, upper white dashed line). At such a segmentation event, I determine the width of the somite, by searching spatially for the steepest point in the signal (Fig. A.7B, blue line). I define that the new segment is formed between the previous boundary of the 'mPSM' and this steepest point, which defines the new boundary of the 'mPSM'.

This very abstract segmentation procedure leads to a pattern that is similar to the one recorded by Lauschke *et al.* (2013), e.g. in their Figure 4a. Also, I calculate somite widths (Fig. A.7C) and travelling wave velocities Fig. A.7 that scale with the shrinking mPSM length,

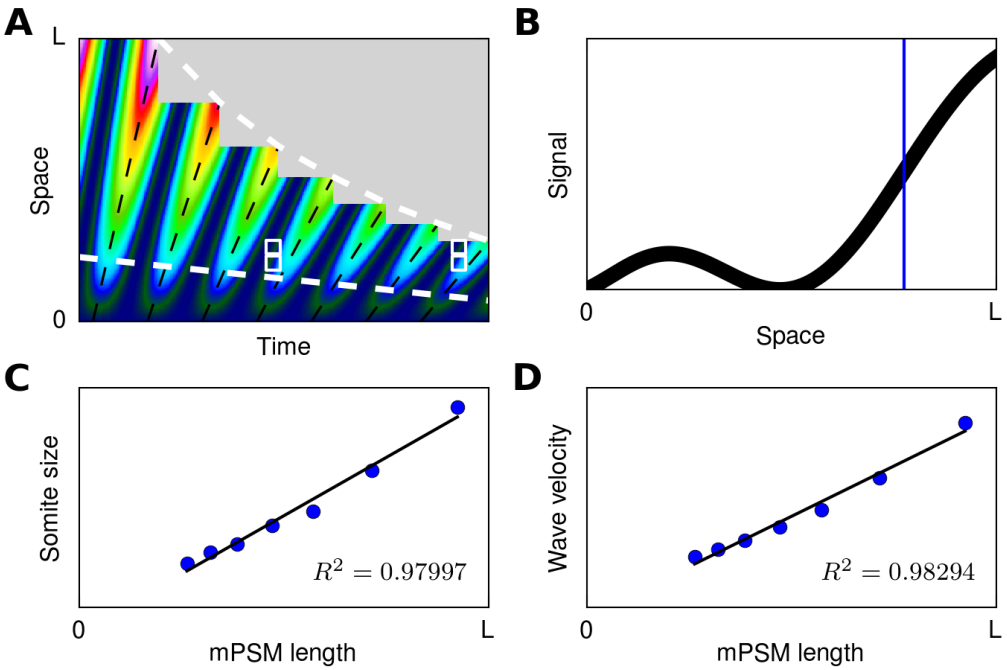

Figure A.7.: **Artificial segmentation leads to scaling in a array of sine oscillators with increasing period and amplitude.** (A) Kymograph of a sine-based model (Eq. (A.2)) of the mPSM. Black dotted lines indicate travelling wave propagation. Upper white dashed line represents the peripheral boundary of the mPSM. Segmentation events are triggered when the peak of the wave reaches this outer mPSM boundary. Lower white dashed line indicates the 'central boundary of the mPSM', when reproducing the experimentally measured phase gradient amplitude of 2π (Lauschke *et al.*, 2013). Phase difference in two neighbouring cells (white squares) increases over time. (B) First segmentation event. The new boundary of the mPSM is defined by the steepest point of the signal in the mPSM. (C,D) In our segmentation model (A), somite size (C) and wave velocity (D) scale with the length of the shrinking mPSM, as observed experimentally by Lauschke *et al.* (2013).

similar to the results shown in the Figure 3a,b of Lauschke *et al.* (2013). The measured phase gradient amplitude of 2π mentioned above, could be explained in two ways. Either by moderate growth (Fig. A.7, lower white dahed line) at the center, which corresponds to the posterior PSM boundary *in vivo*. Or, when considering Figure S5 of Lauschke *et al.* (2013), it could be that this 2π phase span arises from the method of measurement: it is not entirely clear, how the phase gradient amplitude is measured by Lauschke *et al.* (2013).

What are the biological implications of these considerations? In my opinion, there is a strong indidcation that the travelling waves in the mPSM/PSM are shaped by what I call the 'pendulum wave effect': two cells that are initially in-phase, but have a different period, are accumulating phase difference in time. I.e., in the mPSM, the phases of two neighbouring cells that are aligned on the medio-lateral axis, are gradually getting out of phase over time

(Fig. A.7A, white cells). The same is observed *in vivo*: cells aligned on the posterior-anterior axis increase in phase difference as they approach the anterior boundary. This is reflected in the width of the travelling wave stripes (i.e. the wavelength, which decreases towards the anterior (Palmeirim *et al.*, 1997; Jiang *et al.*, 2000; Giudicelli *et al.*, 2007).

In vivo, decreasing wavelengths of travelling waves have been also reported and are referred to as the Dynamic Wavelength effect (Soroldoni *et al.*, 2014; Jörg *et al.*, 2015). To what degree the 'pendulum wave effect' contributes to the *in vivo* Dynamic Wavelength effect is not clear to me, at the moment. A possibility that would explain the *in vivo* Dynamical wavelength effect is scaling of the period gradient: A period gradient which becomes steeper in time leads to a larger period difference in two neighbouring cells that are aligned on the posterior-anterior axis. Consequently, the phase difference in these two cells accumulates faster with a steeper period gradient, leading to decreasing wavelengths of the travelling waves. Interestingly, in our very abstract model, such a scaled period gradient is not needed for the *ex vivo* segmentation.

In our model, the period gradient is static on a domain with static cell. This would imply that the dynamics of the oscillators are controlled by positional information — not temporal information (see Section 4.2).

The biological link of the travelling wave pattern to the segment formation remains elusive (Lauschke *et al.*, 2013; Shih *et al.*, 2015). The results of Shih *et al.* (2015) show that the arrest of the cellular oscillators, which underlay the travelling wave, is initiated at the posterior boundary of the forming somite $S0$ (Fig. 1.1). In my sine-based segmentation model, this posterior boundary of $S0$ is defined via the spatial derivative of the travelling wave signal (Fig. A.7B). Biologically, 'sensing' the spatial derivative of the signal in an array of static cells could suggest that oscillation coupling is involved in the segment formation. However, oscillation arrest and segmentation occur in Notch pathway mutants, where coupling is interrupted (Jiang *et al.*, 2000; Liao & Oates, 2016), discouraging this interpretation.

In summary, my model suggests that the scaling of the phase gradient in the *ex vivo* segmentation process reported by Lauschke *et al.* (2013), does not necessarily require a scaled period gradient. According to this model of sine-based static oscillators, two mechanisms are involved in phase gradient scaling. Firstly, a physical property of oscillator arrays with static period gradients, referred to as the 'pendulum wave effect', which leads to an decreasing wavelength of travelling waves on a static domain, in time. The model suggests that the period gradient is controlled by positional, not temporal, information. For instance, the time delay gradients (see Section 4.2) could be controlled by a morphogen source in the center of the mPSM, representing the tail bud *in vivo* — contrasting with the hypothesis of a temporally 'gradient by inheritance' (see Section 4.2). Secondly, a phase-gradient-linked segmentation process is responsible for the shortening of the PSM length. My model uses information of the spatial signal derivative to establish the link between the phase gradient and the segment formation. It remains open, if this is the only mechanism that can qualitatively reproduce the experimentally observed scaling.

These results and considerations are preliminary and highly hypothetical.

A.4. Data availability

The python code is available on my GitHub repositories.

Code for the *her1* model (main and supplementary figures):
`https://github.com/ttomka/her1_somitogenesis`

Code for the models of *ex vivo* scaling:
`https://github.com/ttomka/ExVivoScaling_Somitogenesis`

Eidgenössische Technische Hochschule Zürich
Swiss Federal Institute of Technology Zurich

Declaration of originality

The signed declaration of originality is a component of every semester paper, Bachelor's thesis, Master's thesis and any other degree paper undertaken during the course of studies, including the respective electronic versions.

Lecturers may also require a declaration of originality for other written papers compiled for their courses.

I hereby confirm that I am the sole author of the written work here enclosed and that I have compiled it in my own words. Parts excepted are corrections of form and content by the supervisor.

Title of work (in block letters):

Travelling waves in somitogenesis: collective cellular properties emerge from juxtacrine oscillation coupling

Authored by (in block letters):

For papers written by groups the names of all authors are required.

Name(s):	**First name(s):**
Tomka	Tomas

With my signature I confirm that

- I have committed none of the forms of plagiarism described in the 'Citation etiquette' information sheet.
- I have documented all methods, data and processes truthfully.
- I have not manipulated any data.
- I have mentioned all persons who were significant facilitators of the work.

I am aware that the work may be screened electronically for plagiarism.

Place, date	**Signature(s)**
Basel, 12.4.2017	

For papers written by groups the names of all authors are required. Their signatures collectively guarantee the entire content of the written paper.